VIRTUAL RADIATION FIELDS FOR ALARA DETERMINATION

By

TRAVIS WARREN KNIGHT

A THESIS PRESENTED TO THE GRADUATE SCHOOL
OF THE UNIVERSITY OF FLORIDA IN PARTIAL FULFILLMENT
OF THE REQUIREMENTS FOR THE DEGREE OF
MASTER OF SCIENCE

UNIVERSITY OF FLORIDA

1995

DISCLAIMER

To my parents,
Dannis and Frances Knight

ACKNOWLEDGEMENTS

While it is certainly true in academia, it can also be said for any sector of the modern world that nothing significant is ever accomplished alone. For this reason, the author wishes to acknowledge the patient advice and trenchant instruction of Dr. G. R. Dalton in making this research possible. His instruction in matters of radiation transport, shielding, and geometrical relationships was an enormous resource toward the development of this thesis.

A debt of gratitude is also owing to Prof. J. S. Tulenko, for his enthusiasm in the study and interest in the author's professional development. Furthermore, the author wishes to thank him for introducing the topic and for the invaluable direction he provided.

Without the efforts of Mr. D. E. Haddox, the VRF program would not have the graphical display and interface that are essential to a virtual dosimetry simulation. His design and implementation of the IGRIP workcell and GSL program made the realization of a virtual dosimeter possible. In addition, the author wishes to thank him for being receptive and helpful with questions regarding computing and simulation techniques.

This research was performed under appointment to the Applied Health Physics Fellowship Program administered by Oak

Ridge Institute for Science and Education for the U.S. Department of Energy.

TABLE OF CONTENTS

Abstract of Thesis Presented to the Graduate School
of the University of Florida in Partial Fulfillment of the
Requirements for the Degree of Master of Science

VIRTUAL RADIATION FIELDS FOR ALARA DETERMINATION

By

Travis Warren Knight

December 1995

Chairman: Dr. G. R. Dalton
Major Department: Nuclear Engineering Sciences

As computing power has increased, so too has the ability to model and simulate complex systems and processes. In addition, virtual reality technology has made it possible to visualize and understand many complex scientific and engineering problems. For this reason, a virtual dosimetry program called Virtual Radiation Fields (VRF) is developed to model radiation dose rate and cumulative dose to a receptor operating in a virtual radiation environment.

With the design and testing of many facilities and products taking place in the virtual world, this program facilitates the concurrent consideration of radiological concerns during the design process. Three-dimensional (3D) graphical presentation of the radiation environment is made possible through the use of IGRIP, a graphical modeling program developed by Deneb Robotics, Inc. The VRF simulation program was designed to model and display a virtual dosimeter.

As a demonstration of the program's capability, the Hanford tank, C-106, was modeled to predict radiation doses to robotic equipment used to remove radioactive waste from the tank. To validate VRF dose predictions, comparison was made with reported values for tank C-106, which showed agreement to within 0.5%. Graphical information is presented regarding the 3D dose rate variation inside the tank.

Cumulative dose predictions were made for the cleanup operations of tank C-106. A four-dimensional dose rate map generated by VRF was used to model the dose rate not only in 3D space but also as a function of the amount of waste remaining in the tank. This allowed VRF to predict dose rate at any stage in the waste removal process for an accurate simulation of the radiological conditions throughout the tank cleanup procedure. Cumulative dose predictions for tank cleanup range from 6.98E+3 to 4.80E+4 rad-SiO_2 (expressed as dose to semiconductors since they are most vulnerable to radiation damage) for cleanup periods lasting from 15 days to 90 days. However, more importantly, simulations permitted the study of shielding effects on cumulative dose. These showed a possible 39% dose reduction for simply shielding the robotic equipment during idle periods.

Additional areas of investigation are presented to illustrate VRF's use as an effective tool in keeping radiation exposure ALARA (as low as reasonably achievable).

CHAPTER 1
INTRODUCTION

Increasingly, the solutions to scientific and engineering problems are yielding to computer simulation and graphical display of the processes, systems, and phenomenon that constitute the particular question at hand [Dur95, Sch95, Vir95]. Their utility is clearly visible for large scale, complex design problems, which are common to nuclear engineering and related fields of the radiation sciences [Dal91]. This simulation based design and modeling is made possible through three-dimensional (3D) modeling and display of a synthetic (computer-generated) workspace also called a virtual environment. Moderate size projects or facilities may be modeled by a single user with a workstation. Modeling or design of larger projects of great complexity can take place over a distributed network of computers permitting many specialist to work together in a common virtual environment [Ang94].

Beginning in 1989, the U. S. Department of Energy initiated an effort to decontaminate and decommission 111 inactive sites [Mur94]. This effort to cleanup contaminated sites is expected to take thirty years lasting until the year 2019. Especially for the more radioactive facilities, a need

exists for accurate predictions of the radiation fields at these environmental and waste management sites. This need can be fulfilled through computer simulation of the 3D environment and its associated radiation fields. Combining such a simulation with a 3D graphical display of the virtual environment would be tantamount to the development of a virtual dosimetry engine, expanding on terminology borrowed from the field of virtual reality (see Figure 1-1 as an example). Therefore, it was the goal of this research to develop a virtual dosimeter that may be applied to the task of predicting radiation doses to robotic equipment and personnel that might operate in a radiation environment.

Virtual Dosimetry Applications

Dose predictions are useful to engineers and specialist for the planning of work performed in high radiation areas. For exposure of robotic equipment, the primary concern is radiation damage to electrical components (mainly semiconductors), which eventually results in failure of these components [Hin90]. Accurate dose predictions can prevent unanticipated failures of equipment inside high radiation areas, which may result in loss of the equipment or unnecessary exposure of personnel in its retrieval. Through the testing of electrical components, engineers have determined the radiation failure threshold for various components as well as their radiation hardened counterparts

[Hin90, Jon95]. Combining this knowledge of failure level with the predicted dose rate for a given task, one can predict the time until equipment failure. This allows the equipment to be retrieved before failure so that it can be repaired and reintroduced to the environment.

For exposure of personnel, the concern lies in limiting the exposure an individual receives to acceptable levels as specified in regulations and facility specific rules. These dose limits are for preventing demonstrable radiation health effects and limiting the risk of latent stochastic effects from biological radiation damage. Consequently, dose predictions for high radiation environments are important for the planning of personnel entries that may be necessitated on occasion. Useful predictions might include how long an individual may stay in the area and how many personnel are needed to perform the task while keeping individual exposures below the set limits.

Finally, a virtual dosimeter can play a large role in support of ALARA (as low as reasonably achievable) programs by aiding in the design and development of radiation shielding and the planning of facility layout. Such programs seek to maximize dose reduction to the extent that is practically possible, consistent with economic as well as health and safety goals [Sch92, Sin91]. While the term ALARA connotes dose reduction for personnel over what is mandated by regulations, it can also be applied to dose minimization for

robotic equipment exposures. Here, the cost of dose reduction must be offset by an equal or greater economic benefit of longer operating cycles and fewer equipment repairs. Computer simulation using a virtual dosimeter will permit the examination of a broad number of designs for dose minimization and ALARA determination.

Advantages of A Graphical Computer Simulation

Traditional computer applications for dose and dose rate prediction problems usually involve the preparation of input files, which are submitted to a program for calculating a set of numerical results. To visualize this output, it must then be transformed into charts or other graphical aids. This can be time consuming and the steps needed to produce the visual aid may distract the engineer from focusing on the problem to be solved. Furthermore, the standard two-dimensional presentation format is often not suited for visualizing multivariate or multidimensional data.

However, 3D virtual environment simulations have demonstrated their usefulness for scientific visualization of these more cumbersome data sets [Dur95, Ill94, Pim93]. Their superiority is threefold with the ability to control the time step or time warp scale factor from within the simulation, alter simulation parameters and model variables on-the-fly, and directly observe the evolution of model variables through the application of graphical objects called "glyphs" [Cra90b,

Ill94]. This later advantage utilizes graphical representation such as color, brightness, size, shape, and spatial orientation to convey information. These graphical parameters are "tagged" to simulation variables forming a graphical coding scheme that maps the computed numerical model into graphical objects that can be seen and readily understood [Pre94]. Such visual cues can alert the user to details, defects, or subtleties in the data that might otherwise have gone unnoticed.

These features all combine to provide a more natural setting for the engineer to explore the problem providing an opportunity to learn directly from the simulation. The engineer is then free to focus all cognitive and intuitive abilities to bear on the problem at hand, while not being constrained or distracted by unnecessary steps. This increases the likelihood that the engineer will find the optimum solution.

An additional advantage of computer simulation is that often the simulation software can draw on existing computer-aided design (CAD) models or databases of a site or facility [Dal90, Ang94]. This linkage with other areas of the design process facilitates the concurrent consideration of radiological design aspects along with the other important design parameters. In addition, this linkage allows the model of the environment to be continuously updated as modifications are made in the real world.

Scope and Objectives of A Virtual Dosimeter

The objective then of this research is the development of a virtual dosimeter that can be used for 3D graphical display and analysis of radiation environments. In particular, this work involves the creation of a virtual dosimetry computer program, VRF (virtual radiation fields), for predicting doses and dose rates in a 3D virtual radiation environment. It is be able to handle complex arrangements of sources, shields and other objects that might comprise the virtual environment, while being capable of calculating the dose rate at any 3D location based on the arrangement. To facilitate an interactive approach with the user, it must be fast to permit updating of the dose rate in real time as changes are made to the virtual environment. Furthermore, for the purposes of dosimetry, it must be able to calculate the cumulative dose to a virtual robot or person performing a given task in the virtual environment.

Tank C-106 of the Department of Energy's Hanford Site was the radiation environment modeled throughout VRF's development (see Figure 1-1). It is a large underground tank containing radioactive waste in both sludge and saltcake forms. Proposals for the remediation of the waste in this and other tanks call for robotic equipment to operate inside the tanks with their associated radiation fields [Har93c, Har93d, Cra90a]. Tank C-106 is discussed in greater detail later in Chapter Four.

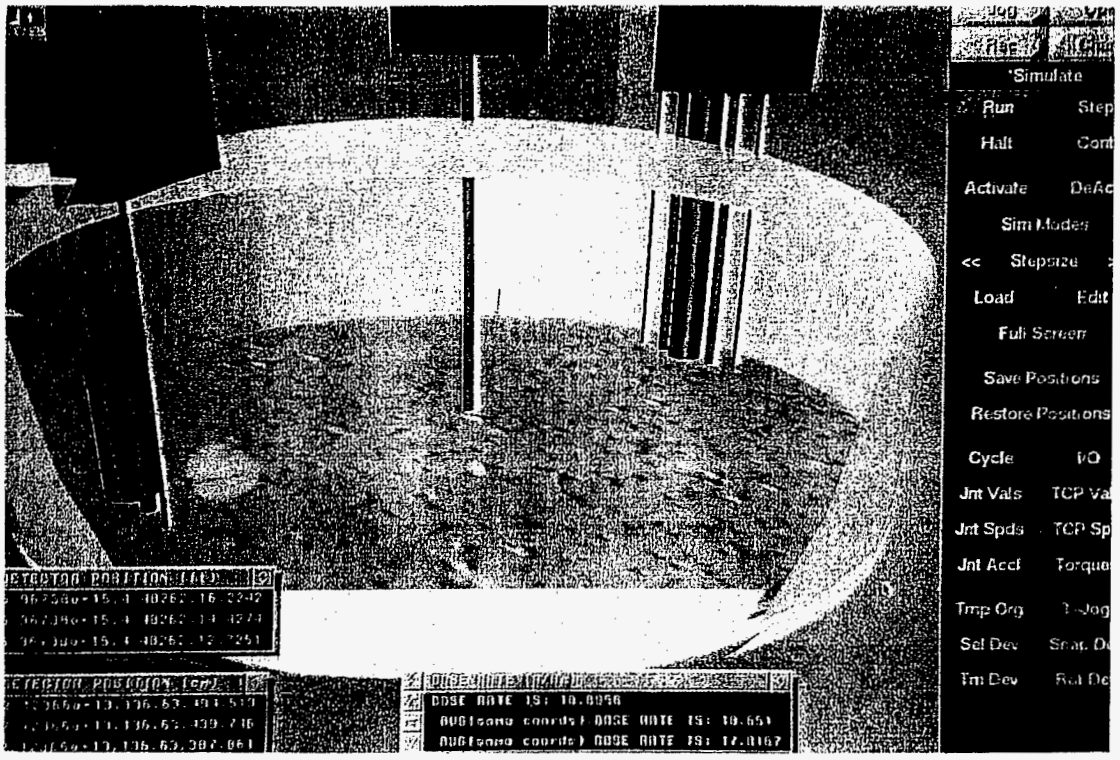

Figure 1-1. The 3D virtual environment of tank C-106. Windows display dose rate and position information for a virtual detector. The virtual environment is displayed using the graphical software, IGRIP®.

CHAPTER 2
REVIEW OF LITERATURE

Review of Current Methods for Dose Rate Calculation

At present, the available computational tools for dose rate calculation and dose rate mapping are predominately nongraphical and input driven. This means that the user must supply all the necessary information (input) before the program will execute and output the desired numerical results. If the user decides to investigate the effects of a parameter on the output then the changes to input must be made and resubmitted to await the calculated result. With each iteration, the user must interpret the output either directly from the numbers if possible or go through the process of constructing a graphical aid, such as isodose curves or a dose rate profile [Bog93, Rai90, Rai93]. The former choice of direct numerical interpretation leaves the user open to misreading the output or overlooking some important trend or anomaly in the data, while the latter adds an additional step delaying the results. For this reason, nongraphical, input-driven codes do not lend themselves to interactive sessions where the user makes effective use of the computer feedback to fully explore the problem. The utility of a more interactive working session with the computer will be discussed in greater

detail in the section titled "Virtual Environment Principles" later in this chapter.

The current, input-driven computer programs make it difficult to accurately model the duty cycle of robotic equipment or personnel in a radiation environment. To predict cumulative dose, the dose rate must be requested by the user at discrete points throughout the duty cycle and combined with foreknowledge of residence at these locations. The alternative is to calculate average dose rates for selected general areas simplifying the calculation. Either method is clearly inferior to the three-dimensional, computer-controlled simulations proposed by this research.

An improvement over the non-graphical, input-driven software are computer programs such as Microshield®, which employ some graphical capabilities and respond to the user in an event-driven mode [Mic88]. Generalized, graphical images of various source/shield geometries are used to help the user visualize the model's setup. Here, the user is limited to a select few geometries, which are not displayed to scale and are only representative of the environment being modeled. Moreover, only one source can be modeled at a time so that each source must be modeled separately and their contributions summed by hand.

However, the event-driven method of data entry is a vast improvement over the input-driven method. The user is presented a data entry screen with locations for each input

variable along with prompts for identification. This reduces the chance of getting the data out of order and the wrong value being assigned to a variable. Also, each value may be checked as it is entered to see if it conflicts with other data supplied by the user and to alert the user to a possibly erroneous entry.

However, similar to the other computer programs, no method exists to calculate cumulative dose to a robot or person that might be working in that environment. Also, only numerical output is available to the user with no graphical visualization aides. The program does allow for sensitivity analysis of an input variable to study its effect on the model. However, the user must still interpret the numbers or construct a graphical image to better observe any trends.

To automate this process, some computer codes have been written whose sole function is to collect data output from a computer program and generate graphical aids. McIntyre et al. describes a set of subroutines called HANDYPACK that generates histograms from data output by the EGS4 computer program, a Monte Carlo simulation code for electron and photon transport. Still other routines have been designed to view particle trajectories from Monte Carlo simulations [McI90]. While only two-dimensional graphics are presented, these graphical tools have proven useful for optimizing certain applications and providing a better understanding of the relationship between radiation interactions and the resulting dose distributions.

To date, there has been extensive work in the field of robotic simulation using virtual environments for mobile and semiautonomous robotic control [Cra90a, Cra90b, Had94]. However, there has been no application of virtual environment simulation and dose rate prediction to dose assessments for the robotic equipment. Knowledge of the virtual environment allows the robot to plan its action, while the user can preview those plans through a graphical user interface that displays the virtual environment. A virtual dosimetry application makes use of this same virtual environment and graphical user interface. To predict radiation doses, radiological data collected or estimated from the real world is added to the computer model. The virtual dosimetry application would give the added ability to calculate radiation doses ahead of time for a given set of actions also called a duty cycle. Thus allowing the robot to also select the path for which it would receive the least dose. Virtual reality technology represents a fresh approach to this engineering problem, while automating the procedure necessary to obtain accurate predictions.

Review of Virtual Environment Principles and Components

Virtual Environment Principles

A virtual environment can be described as an immersive and interactive synthetic world generated by a computer. However, this terse definition belies the true importance of

computer-driven virtual environment simulations for exploring complex engineering problems. To understand this, it is necessary to explore the key adjectives of immersive and interactive.

Immersion. Immersion gives the user the ability to focus on the problem or issue that is being investigated with virtual environment technologies. The more natural and unobstructed the user interface, the higher the degree of immersion the simulation will allow. For this reason, higher-end virtual reality systems are very immersive since the user is projected into the environment using multiple forms of feedback including stereoscopic images, three-dimensional (3D) sound, force feedback, and tactile simulation.

For engineering applications and scientific visualization, it is not necessary for the computer to generate a totally believable alternate reality. This is especially true when modeling abstract principles and phenomenon such as radiation, for which we have no natural perception. Instead, the importance of scientific immersion lies in how well the user is able to selectively focus on the process or phenomenon under investigation. Preece et al. describes these simulations as model-based visualizations, whereby the user interfaces with the computer directly controlling the evolution of computer-based models [Pre94]. The utilization of a graphical interface permits the seamless mapping of the underlying computer model to a graphical form

that can be readily understood. In this way, virtual environment modeling prevents the visualization medium from obstructing the user's perception and allows for the selective focusing that is needed for complex problems.

Virtual environments achieve this more immersive, natural approach to problem solving in two ways. First, they are three-dimensional. Because simulations can evolve over 3D space as well as time, a 3D display is more appropriate [Gla95]. In the context of this study, the dose rate at any site will vary in three dimensions for even simple arrangements of sources and other objects including shielding. Therefore, a 3D-dose-map display provides a more natural medium for the user and presents the information with greater clarity than any two-dimensional display.

Secondly, virtual environment simulations use a graphical coding scheme to map the numerical computer-model into a graphical presentation for the user to visualize [Pre94]. This coding scheme tags parameters or variables of interest using graphical objects called "glyphs" to graphically represent their value. The user can then observe these graphical objects evolve as the simulation progresses in time and/or space. Some methods of graphical coding include variation of color, brightness, size, shape, and spatial orientation [Ill94]. A good graphical coding scheme becomes more important as the model grows in size and complexity. A user can comprehend much more information in a shorter amount

of time graphically than by staring at many numbers. Also, graphical coding reduces the chance that an anomaly, defect, or other subtle detail in the data might go unnoticed.

Interaction. In addition to allowing a high degree of immersion, virtual environment simulations are also very interactive [Dur95]. The user can respond to the virtual experiment in real time much as he would to an experiment in the real world. Because the simulation is interactive, a virtual feedback loop is established between the computer and the user. The user makes use of this feedback to control the direction of the experiment [Pre94]. Various interactions of the user with the virtual environment via the graphical user interface can be classified according to function, each with particular advantages over nongraphical, input-driven computer modeling and real world experiments. The first is the ability of the user to control the time step or time warp scale factor [Cra90b]. This allows the simulation to proceed slower or faster than real time or even to replay a sequence over again, which is important in allowing the user to learn and gain insight from the model.

Secondly, because the simulation is a 3D representation of an environment, the user can navigate through the environment to obtain a different view point. Not only can any perspective be achieved, the user can even pass through objects that might otherwise obscure a particular view. Indeed, virtual environment simulations make possible views

that simply cannot be achieved in the real world such as observing the flow of water from within the channel without interfering [Egg94].

Another type of interaction available in a virtual environment simulation is control of model parameters and simulation variables. Controls such as graphical icons, buttons, slide bars, and other "widgets" are accessible graphically within the simulation [Bra92]. This makes it very simple for the user to alter the simulation on-the-fly without interrupting its progression. Utilization of these graphical tools permit the user to directly observe the effect a model parameter has on a simulation variable. The user can control experiments in the virtual world by controlling the conditions of the simulation.

Finally, the user may also change the way that the underlying computer model is visualized or "mapped" in the simulation [Pre94]. This allows the user to optimize the graphical display and select a graphical coding scheme that best illustrates the model. Typically, a change in the coding scheme is a more involved process and likely results in significant interruption of the simulation and the user's immersion. However, all of the interactive features mentioned above serve to place the user in control of the simulation. This is a remarkable improvement over nongraphical, input-driven computer models, where control is highly structured and the expression of model variables and relationships is

severely limited. Computer based visualization using virtual environment technology can be applied to scientific and engineering problems to "make perceptually prominent those things [elements and relationships] that we wish to be conceptually prominent" [Pre94, p. 242].

Components of A Virtual Reality System

From discussing the principles governing a virtual reality system above, it should be clear that such a system interfaces very closely with its user to achieve its immersive and interactive nature. This leads to the major division between the components of a virtual reality system. The two major components that comprise a virtual reality system are the sensory effectors and the reality engine [Pim93]. Sensory effectors form the physical interface between the user and the computer. They are the instruments and peripherals the computer uses to provided sensory information or output to the user and provide feedback from the user as input to the simulation [Sad94]. An example of an effectors is a head mounted display (HMD). This device is worn like a helmet and is equipped with a separate LCD screen for each eye providing stereoscopic images of the virtual world. The HMD also is used to track the user's head movements and adjust the display to match the direction being observed. So the HMD serves both as a sensory output and feedback effector.

The reality engine is the software and computer hardware that is responsible for conducting the simulation based on the underlying computer model and user feedback. It generates all the sensory output to provide and maintain the user's sense of presence in a virtual world. The reality engine itself can be divided into three components based on function. Each of these components will be discussed here since they are essential to any virtual reality system including a virtual dosimetry application.

Application software. The application software determines the character and purpose behind the simulation such as whether it is a flight simulator or a virtual wind tunnel. It describes the dynamics of objects in the virtual environment and both allows and limits their interaction with each other and with the user. Some examples might include if and how an object moves and whether it interacts in some prescribed manner or only when acted on by the user. In a sense, it is like the governing physical laws for the virtual world. The application is essential to making virtual reality interactive beyond simple navigation through a static virtual world. The application software can be operated on by the user to explore and collect information about the virtual environment. It controls and limits the conducting of virtual experiments by the user within a framework that is set by its programming.

Geometry database. A database of virtual objects is necessary for the reality engine to call upon when the application is initiated or when the user signals for another object to be added to the simulation. The database includes such information as shape, color, texture, or other attributes necessary to fully experience each object. This information is used to display the object as well as determine other qualities of how it may be experienced by the user through some effector. Other information might be required by the application software to determine how each object interacts with its virtual environment.

Simulation manager. The simulation manager coordinates all the various pieces of hardware, software, and database to generate the virtual reality experience. Its performance is vital to promoting the user's immersion in the virtual world. It must be capable of updating the virtual world at least ten times every second to prevent the user from experiencing nausea from lags in the virtual display corresponding to the user's head movements [Tau94]. Therefore, the capability of the simulation manager is directly tied to the computing power of the PC or workstation.

CHAPTER 3
METHODOLOGY

Components of the Virtual Dosimeter

In the above review Of virtual reality systems, three necessary components were identified--the simulation manager, application software, and geometry database. Each of these components are also necessary for a virtual dosimeter. Figure 3-1 illustrates the functional relationship of each component with the arrows indicating data streams or flows between components.

IGRIP--The Simulation Manager

The three-dimensional (3D) graphical modeling program known as IGRIP® (Interactive Graphics Robot Instruction Program) by Deneb Robotics Inc. was selected to be the virtual dosimeter's simulation manager. In IGRIP terminology, the virtual environment being modeled is called a workcell, which is composed of individual virtual objects called devices. A robot is an example of a complex device with many moving parts. A computer-aided design (CAD) component of IGRIP allows the user to construct each individual part from simple geometrical objects called CAD primitives. The virtual objects used in this study are quite simple such as

cylindrical, annular, and box shaped sources and disk shaped shields. However, IGRIP's ability to deal with more complex devices means that it can keep pace as more detail is added and virtual environments become more complex. Indeed, IGRIP is most often used for the simulation and control of robots both in the virtual world and the real world. Using these simulations as a starting point, the VRF program could be operated simultaneously to provide dosimetric information for robot simulations.

Perhaps IGRIP's most obvious role in virtual dosimetry is to provide a visual display of the 3D virtual environment. Through a graphical user interface (GUI), the user can maneuver devices, navigate through the workcell to obtain the desired view point, and extract information about the various objects including collision detection and clearance [Had94, Dal91]. This information is useful for the control or monitoring of robots as they move through complex radiation environments.

To make the virtual dosimeter interactive, the GUI is customized to the virtual dosimetry application. IGRIP's graphical simulation language (GSL), a high level Pascal-like programming language, is capable of generating popup menus for entering data or commands or displaying simulation variables. Output of the VRF code is displayed in a GSL popup window. For example, during a simulation, the local dose rate and a receptor's cumulative dose are displayed along with its

current position. In addition, a popup menu could replace the VRF menu-driven interface to provide a unified GUI for virtual dosimetry simulations.

This two way communication between an IGRIP GSL program and the Virtual Radiation Fields (VRF) code is made possible via a socket. Sockets are a method of communicating streams of data or commands between a client and a server. It is used by IGRIP to update the VRF code on the location of a dose receptor in the virtual environment. A GSL program sends the location data for the receptor, which may represent a person or a robot, each time the receptor moves a set distance away from its last position (see "Cumulative Dose Calculations" later in this chapter). VRF returns the dose rate and cumulative dose for a virtual receptor in an IGRIP simulation.

VRF--The Application Software

The responsibility for calculating the dose rate at any point in the 3D virtual world falls to the VRF computer code, which was written in C and conforms to the ANSI C standard. Calculations are performed based on the given knowledge of the virtual environment such as the strength and arrangement of the radiation sources. For previously created virtual environments, this information is read from a file when the program is initiated. Additions, deletions, or changes made by the user through IGRIP's GUI can be updated in the VRF program via a socket. Another task of the VRF code is to manipulate

the radiological data--attenuation coefficients, activity, etc.--concerning each virtual object. This information is necessary for calculating the dose rate and is also contained in the virtual environment file. If new objects are to be added during a simulation, the user must supply this data.

The VRF code initiates a new dose rate calculation whenever the GSL program transmits a new set of coordinates for the dose receptor via the socket. Once the dose rate is calculated it is sent back through the socket. The GSL program displays the new dose rate and the receptor's position in separate popup menus. Cumulative dose can also be calculated and monitored by the VRF code. This is discussed at length in this chapter under the section, "Cumulative Dose Calculations."

Virtual Objects--The Geometry Database

For a virtual dosimetry application, the types of objects that might be found in the virtual world can naturally be divided into three classes--sources, structures, and receptors--according to their function. All information regarding each individual object is stored in a separate C structure variable not to be confused with structure type virtual objects. This information is read from the virtual environment file at the start of the simulation and is updated as changes are made to the virtual environment. The C structure variables are a convenient form to represent

different variable types that are associated with a particular entity or record in this case a virtual object. The most basic information contained in these variables relates to the object's geometry and position in the virtual environment. Accordingly, the C structure variables and the virtual environment file function as the geometry database of the virtual world.

Each virtual object regardless of classification must be described by the fundamental object parameters of geometrical type (shape), dimensions, location in the virtual environment, and orientation with respect to the virtual environment's coordinate system. Table 3-1 lists the various types of geometry useful to virtual dosimetry applications, however not all types are available as both sources and structures. There are certain commonalities and fundamental differences between the different types of virtual objects. These will be explored next so that their roles in dose rate calculations will be clear.

Structures. Shields, walls, and hardware are some common examples of virtual structures. Whether intentional, as in the case of a shield, or not, all structures attenuate incident radiation to some degree. However, depending on their size, attenuation coefficient, density, and placement in the virtual environment, they may or may not significantly reduce the dose to a receptor. The various data fields in the geometry database relating to geometrical type and size must

be supplied if they are to be considered for receptor dose reduction by the VRF code. In addition to the fundamental object parameters, coefficients for radiation attenuation and buildup must be provided. This data must be supplied at discrete photon energies over a range sufficient for the code to interpolate for the specific gamma-ray energies emitted by the virtual sources.

Sources. This class of virtual objects is unique in that sources emit radiation and are therefore of principal concern to the user. In addition, they attenuate radiation originating in themselves (self-shielding) and also incident radiation from other sources in the virtual environment. While any source of complex shape and composition can be accommodated using a sufficiently complex mathematical description, only non-reentrant, geometric shapes of uniformly distributed composition are considered to simplify the necessary computations. Specifically, for an object to be non-reentrant, it must not be possible to extend a vector from any point inside the object, exit the object at some point, and then reenter the same object at a later point along the same vector.

Similar to structures, information on sources must include their fundamental object parameters as well as data on radiation attenuation and buildup. In addition, virtual source information must include all gamma-ray energies, their

intensity (percent yield per decay), and the overall source activity.

Receptors. A virtual receptor can be any object for which the user wishes to collect dosimetric information. It could be a virtual detector that the user moves about the virtual environment to obtain a dose rate readout. A virtual receptor can also represent robotic equipment or personnel. Here the user may also be interested in cumulative dose prediction as well as dose rate. While receptors are considered as virtual objects for organizational purposes, their treatment by the VRF program is very different. As will be seen in the next section on dose rate calculation, the dose rate for a receptor is calculated at a single point. Therefore, the dimensions of a receptor are not as important as its 3D location, which is the only physical receptor parameter utilized by the VRF program. Also, since receptors are likely to vary in shape and dimensions more than sources and structures, the simple geometrical shapes are not adequate for their display. If the user wishes, a more realistic and complex image can be displayed by IGRIP instead of a symbol used to represent the receptor's location. Either way, the dimension, orientation, and geometry data in the C structure variables are not utilized by the VRF program for a receptor.

Attenuation of radiation by receptors is not considered since they are very mobile and it is not likely that they would provide significant shielding for other receptors.

However, one additional radiological parameter is necessary for virtual receptors. A material dose conversion factor should be supplied to convert the exposure dose (units of roentgen) calculated by the VRF program into absorbed dose to the receptor material expressed in rad. For robotic equipment the conversion factor is 0.877 rad-$SiO_2 \cdot R^{-1}$, which is for silicon dioxide since the electronic components are most vulnerable to radiation damage [Att86, Hin90, Ekd91]. The dose conversion factor for humans is usually expressed in terms of dose equivalent, which is related to human-tissue absorbed dose but is weighted to be proportional to the risk of latent stochastic effects such as cancer. For photon energies below 3 MeV, the dose equivalent conversion factor is 0.96 for dose equivalent in units of rem [Cem83].

Computational Method for Dose Rate Calculation

Before exploring various computational approaches to virtual dosimetry, it was necessary to identify the types of radiation to be treated. With the exceptions of particle accelerators and reactor containments during operation, most radiation environments encountered consist of either alpha, beta, or gamma radiation. Based on their ranges and ability to penetrate a receptor, it was decided to only consider gamma radiation.

Because of their mass, alpha particles are the least penetrating with a range of about 3.6 cm in air for an initial

energy of 5 MeV. Their range is even less in tissue and SiO_2 with ranges on the order of micrometers. Being lighter, beta particles have longer ranges varying from tens to hundreds of centimeters in air for those that are very energetic. Since they can penetrate the outer layers of skin, a correction factor may be warranted for situations of close contact with beta emitting sources where no significant attenuation is provided by air. For robotic equipment, the shielding requirements are minimal with a couple millimeters of a material with low atomic number capable of stopping most beta particles. Therefore, because the doses received from alpha and beta particles is expected to be small in comparison to the that received from gamma rays, their effects are not considered in this study.

The overriding considerations in selecting a calculational method where speed and accuracy for complex virtual environments. Clearly, accuracy is important if the predictions are to be of any practical use. Also, computational speed must be considered if the simulation is to maintain an appropriate level of immersion by the user (see the section titled "Virtual Environment Principles" in Chapter 2). Based on these criteria, the computational approach selected for virtual dosimetry is a ray analysis technique using simplified Monte Carlo methods. It begins with the birth of a gamma ray at a uniform and randomly selected location inside the source. This random, uniform birth is

consistent with the stochastic nature of radionuclides and their assumed uniform distribution in the source. More complex distributions of radionuclides in the source material can be handled but only by sacrificing some speed and necessitating some more memory storage. However, distributions that vary according to a moderately simple mathematical formula could be implemented with little additional effort.

Following birth, the gamma ray is then forced to escape the source along a ray or line-of-sight between its birth and the receptor's location so that each gamma ray is incident on the receptor [Chi84]. Differing from full Monte Carlo simulations of the photon's behavior, this ray tracing scheme greatly simplifies the calculation. The gamma ray and the secondary radiations that it generates are not followed through their many complex interactions in the virtual environment. Instead, each primary gamma ray is forced to be incident on the receptor where their probability of incidence (statistical weight) is averaged. This simplified approach should reduce the number of gamma rays that must be sampled since variation between photon interactions and trajectory is removed. Also, the time required for the calculation is reduced by using fewer gamma rays and because detailed information on the scattering of gamma rays is not collected. Because this abbreviated model is not a completely accurate representation, it is necessary to make corrections in order

to obtain total dose rate (see the section titled "Buildup Factor" later in this chapter).

Since the ray analysis method is based on counting photons from individual source locations to a point receptor, each randomly selected birth location can be treated as a point-like source in determining its contribution to the gamma ray flux at the receptor. This individual contribution will vary depending on birth location because of processes such as attenuation and geometrical spreading. Therefore, random selection of birth locations provides an appropriately weighed measure of the gamma ray flux. After the contribution from many such points are averaged, a gamma ray flux at the receptor can be reported.

It is very important to note that the estimated error is based on the variance between individual gamma ray contributions and the sample size. This allows the Monte Carlo calculation to be terminated as soon as a desired error level is attained.

This treatment of volumetric sources as collections of randomly selected individual point sources is directly analogous to more analytical techniques (point kernel) using differential elements of a source that are integrated over its volume. Since in almost every case an analytical result is not possible, these traditional techniques must resort to numerical solutions and/or approximations. Knowing this, the advantage of using a simplified Monte Carlo approach is clear

especially for complex arrangements of sources and other virtual objects.

To account for each gamma ray's true probability of being incident on the receptor, its statistical weight must be reduced accordingly. Because each birth of a gamma ray is isotropic, its statistical weight must be divided by four-pi steradian to account for the biasing of all photons to be incident upon the receptor. Additionally, since all sources are envisioned as a collection of point sources, the photons obey the inverse square law and their weights are accordingly reduced by the inverse squared distance between birth and the receptor. The gamma ray's weight must also be reduced to account for the exponential attenuation that occurs while escaping the source. For this reason, sufficient data points of the source attenuation coefficient, μ_s, must be supplied over the energy range that might be encountered in the virtual environment. This is a significant computational step since the exit distance, $\underline{d}_{exit}$, must be calculated for each gamma ray sampled by the computer. Here, geometry is important since the equation used to calculate the exit distance will vary with each source geometry.

Furthermore, exponential attenuation through other objects between birth and receptor must also factor into the gamma ray's weight. For a given ray intersecting an object in the virtual environment, there will be a path length, $\underline{d}_k$, through this object that will contribute to the attenuation of

the gamma ray. The VRF program interpolates the attenuation coefficients, μ_k, of all objects and for all gamma ray energies emitted by the different sources based on the data provided for each object. If all these factors that reduce a gamma ray's statistical weight, ω, are collected into one equation,

$$\omega = \frac{e^{-\mu_s d_{exit} - \sum_{k=1}^{m} \mu_k d_k}}{4\pi r^2}, \qquad (3\text{-}1)$$

it is clear that this is the predicted contribution from a single gamma ray to the uncollided fluence at a receptor point $\underline{r}$ distant from a point source.

The method continues to sample gamma rays at random locations from the source calculating their individual weights and summing them together. By dividing by the number of gamma rays sampled, the result is the predicted fluence,

$$\overline{\phi^{uncoll.}} = \frac{\sum_{l=1}^{N} \omega_l}{N}, \qquad (3\text{-}2)$$

from a single gamma ray born at random in the source and incident on an infinitesimal sphere located at the receptor. This sampling continues until the estimated relative error in the calculated fluence falls below a tolerance set by the user. The estimated relative error is given by the expression,

$$\epsilon = \frac{Z_{\alpha/2}}{\bar{\Phi}} \sqrt{\frac{\sigma_{\Phi}^2}{N}}, \qquad (3\text{-}3)$$

which is evaluated for N samples [Shr66]. If the estimated error is too great, additional gamma rays are sampled and the error is estimated again for the total sample. The parameter, $Z_{\alpha/2}$, specifies the desired degree of certainty based on the normal distribution. A value of 1.96 corresponds to the 95% confidence level with smaller values representing lesser degrees of certainty. The user is allowed to set both the relative error limit and the confidence level for all calculations.

Multiplying this predicted fluence by the source activity concentration, A_v, the fraction of gamma rays per decay, f, and the source volume, V, and density, ρ, yields the uncollided flux,

$$\overline{\varphi_{i,j}^{uncoll.}} = f A_v V \rho \overline{\Phi_{i,j}^{uncoll.}}, \qquad (3\text{-}4)$$

where (i, j) indicates the jth energy gamma ray emitted by the ith virtual source. From this calculated flux, a conversion factor, k(E), can be used to obtain the dose rate,

$$\overline{\dot{D}_{i,j}^{uncoll.}} = k(E_{i,j})\, E_{i,j} \overline{\varphi_{i,j}^{uncoll.}}, \qquad (3\text{-}5)$$

to the receptor from the uncollided gamma rays. The dose rate conversion factors used in this study were taken from ANSI/ANS-6.1.1-1977 with dose rate expressed in R/hr [Fod78].

The exposure-dose-rate conversion factors are a function of gamma-ray energy and are tabulated for 0.5 to 10 MeV.

For sources that emit multiple energy photons, a separate calculation must be made for each energy. This is necessary since the attenuation coefficients for the various materials vary with photon energy. Also, the dose conversion factors are different for varying primary photon energy. Once the dose rate is calculated separately for each photon energy, these can be added to obtain the total dose rate from that source. Similarly, the dose rate contribution from each source in the virtual environment must be calculated and added together to obtain the total uncollided dose rate from all sources. Therefore, the total uncollided dose rate,

$$\dot{D}_{total}^{uncoll.} = \sum_{i=1}^{M} \left(\sum_{j=1}^{N_i} \dot{D}_{i,j}^{uncoll.} \right), \qquad (3\text{-}6)$$

can be calculated for $\underline{N}_i$ different energy gamma rays from each of the $\underline{M}$ sources in the virtual environment. This ray tracing approach provides a very efficient prediction of the primary (uncollided) gamma ray flux at the receptor's location. However, much information is lost regarding the true energy distribution of all radiation incident on the receptor. For example, gamma rays are emitted in all directions from the source into the virtual environment. Gamma rays that are emitted in a solid angle different from the one traced to the receptor can be scattered by other virtual objects to the receptor. One form of this dose from scattered radiation is

known as "skyshine" where the scattering medium is the air. However, this contribution is expected to be small since the radiation must travel a larger distance and the scattered and secondary radiations are usually peaked in the forward direction, which would be out of line with the receptor [Chi84]. For scattering angles away from the forward directions, exposure from this component is typically about 200 to 2000 times lower than the directly incident exposure [NCR76]. For most cases, this "object shine" will not make a significant contribution to the receptor's dose and the error in the predicted dose rate is expected to be small.

More importantly however, this approach ignores interactions of primary gamma rays that are emitted by the source in the solid angle about the ray traced to the receptor. Scattered gamma rays of a lower energy are the result of Compton interactions. Secondary radiation such as electrons and positrons are generated by photoelectric and possibly pair production events for more energetic, primary gamma rays. This secondary radiation will further interact to produce tertiary radiation such as photons and electrons. As mentioned above, the radiation produced in these events is emitted with an angular distribution that is highly peaked in the forward direction. The result is a build up of lower energy scattered and secondary radiation that is also incident on the receptor. In many cases, this "buildup" can be a significant contributor to the receptor's dose and should be

taken into account by the calculational method. For a complete discussion of how this is treated, see the section titled "Buildup Factor" below.

A final consideration regarding the calculational approach involves both attenuation and buildup so it is discussed here. The effects of air as an attenuating medium are ignored by the VRF program, which treats these regions as vacuums. This assumption is justified on the grounds that for most radiation environments, air does not play a significant role. For photons between 0.5 MeV and 2.0 MeV, the mean free path in air varies from about 95 meters to almost 190 meters respectively [Fod78]. Most radiation environments that are modeled involve distances much less than this so that attenuation cannot play a significant role compared with geometric spreading and attenuation by other objects likely present. Accordingly, radiation buildup in air would not be significant since buildup is also a function of optical length. For example, 0.6617 MeV photons from ^{137m}Ba (^{137}Cs) traversing 10 meters of air undergo attenuation and buildup with a product equal ~1, which can be neglected in comparison to other calculational uncertainties.

Buildup Factor

As discussed above, it is necessary to treat the build up of scattered radiation in order to accurately predict the total dose rate to the receptor. This is handled by the use

of a multiplicative "buildup factor" that adjusts the uncollided dose rate calculation previously shown in Equation 3-4 to predict the total dose rate. Several empirical functions that fit data from both direct experiments and numerical calculations have been published [Har93a]. Parameters required for these approximations vary with initial gamma ray energy, the elemental type of the attenuating medium, the optical path length of the primary gamma rays in the medium, and the arrangement of the source and the attenuating medium(s) [Chi84].

Because the empirical parameters are functions of so many different variables, sufficient data points must be provided for each parameter for the gamma ray energy range and elemental materials found in the virtual environment. The buildup formulas are setup to calculate buildup as a function of optical path length and are fit to give reasonably valid results for values usually between 0 and 40 mean free paths [Har93a]. Since the computational method used by the VRF code treats extended sources as collections of points, the point-isotropic-source buildup factor data is utilized, which removes any need for further geometric considerations with regard to buildup. A buildup formula can then be applied using point-isotropic-source buildup parameters to calculate the appropriate buildup factor for each ray traced from birth to receptor. Since the buildup factor is a function of path length and path length will vary for each ray, the buildup

factor should be included before the averaging of the gamma ray fluence previously shown in Equation 3-2. Accordingly, the total dose rate,

$$\overline{D_{i,j}}=k(E_{i,j})\,E_{i,j}(\overline{B\varphi})_{i,j} \tag{3-7}$$

can be expressed using a calculated buildup factor, where $(B\varphi)_{i,j}$ is shown to emphasize that it is the product that is averaged by VRF.

While a buildup factor can be defined for various radiation quantities, all dose calculations in the VRF code are evaluated for exposure dose, which is derived for air. This choice is for convenience since the real world comparison study is reported in exposure units. Also, exposure dose is easily converted to absorbed dose in any material by a simple conversion factor for that material (see "Receptors" in the section titled "Virtual Objects" earlier in this chapter).

Harima makes a comparison of several buildup formulas over the range of 0.015 MeV to 15 MeV giving their maximum percent deviation at discrete points over this range [Har93a]. Despite its rather large maximum deviation (as much as 40% in the range of typical energy values), the Berger formula,

$$B=1+\alpha\mu de^{+\beta\mu d} \tag{3-8}$$

was selected for use in the VRF program. It has the advantage of only requiring two parameters, α and β, and also requires fewer operations than some of the more elaborate buildup formulas. While the Taylor formula is similar, it requires

three parameters and its maximum deviation is comparable to that of Berger's formula [Har93a, Chi84].

The above calculated form for buildup is convenient but applies only to the case of a single attenuating object between the gamma rays birth and the receptor. This would be the case for unshielded, optically thick sources where significant buildup can occur in the source material. Additionally, it applies to optically thin sources shielded by one object so that buildup practically occurs only in the shielding object. The difficulty arises in trying to apply the buildup formula to the case of laminated or stratified shields, which might occur in complex virtual environments where the receptor is shield from a source by multiple objects.

The treatment of multiple shielding objects is complicated by the many possible combinations that can exist between number of shields, types of material, ordering, thickness, etc. [Har93b]. Generalizations can be made about how best to apply buildup for a select few arrangements particularly with regard to two shields that differ significantly in atomic number [Chi84]. However, they have a limited scope and lack precise, quantitative rules regarding their application. This makes them nearly impossible to adapt into a computer algorithm for broad application to virtual dosimetry.

More precise, numerical approaches have been tried to deal with this problem. The simplest approach of multiplying the buildup factor for each shield is woefully inadequate. This greatly overestimates buildup by not accounting for the saturating effect of buildup for greater optical thickness [Jae68]. Broder's formula treats the buildup from each successive layer as the sum of the difference between the buildup of that layer for the total depth penetrated and the buildup of that layer for the total depth penetrated up to that layer. This can best be seen in the recurrence relation,

$$B\left(\sum_{k=1}^{M}\mu_k x_k\right)=B\left(\sum_{k=1}^{M-1}\mu_k x_k\right)+\left[B_M\left(\sum_{k=1}^{M}\mu_k x_k\right)-B_M\left(\sum_{k=1}^{M-1}\mu_k x_k\right)\right], \qquad (3\text{-}9)$$

which simplifies for computational purposes to,

$$B\left(\sum_{k=1}^{M}\mu_k x_k\right)=\sum_{n=1}^{M}B_n\left(\sum_{k=1}^{n}\mu_k x_k\right)-\sum_{n=2}^{M}B_n\left(\sum_{k=1}^{n-1}\mu_k x_k\right) [Jae68]. \qquad (3\text{-}10)$$

This method has the advantage of introducing no additional parameters for calculation. Other more accurate methods have been investigated, which yield better results such as Kitazume's formula or Kalo's method for a lead-water shield [Woo82, Jae68]. However, the former requires consideration of an additional parameter with only limited reference values available, while the later option is limited to shielding arrangements of only two materials. Either method does not fit the criterion of being applicable to the many different

combinations of shielding arrangements that might be found in a complex virtual environment.

Despite being convenient and easily applied to any shielding arrangement, Broder's calculation of buildup for multilayer shielding is by no means precise. Chilton describes treatments of laminated shields to be of "dubious merit, for the most part" [Chi84, p. 198]. Broder's method is applied in the VRF program as a practical means of handling some of the complex arrangements that might present themselves. However, it is applied with the acknowledgement that its development is more practical than theoretical and ultimately recognizing the limitations of the ray analysis method. For increasingly complex radiation environments or if greater accuracy is required, a more exact computational method should be adopted.

A further consideration regarding the accuracy of empirical buildup factors relates to the shielding object's geometry. Most of the available buildup data was evaluated for an infinite shielding medium instead of the finite geometries that are found in the real world. Application of infinite-geometry buildup data always results in an overestimation of the dose and more significantly so for low energy photons and shields of low atomic number [Woo82]. Correction factors for finite geometries are available for some shielding materials [Jae68]. However, with the above noted exceptions for low energy and low atomic number, the

error is small and the correction factor approaches unity for increased shield penetration. Additionally, this overestimation of dose may allow for some error cancellation with reflected scatter, which also is not taken into account and would underestimate the total dose (see "Computational Method for Dose Rate Calculation" earlier in this chapter).

Cumulative Dose Calculations

Thus far the discussion has centered on the dose rate computational methodology. However, to make cumulative dose predictions for given tasks requires information regarding receptor location and time spent in the radiation environment. In virtual dosimetry, this information is supplied through the simulation of the receptor as it executes what is called a duty cycle. Practically speaking, a duty cycle is a data set that traces the receptor in both three-dimensional space and time for performance of a given task. This could consist of a singular task for which the user is interested in predicting cumulative dose. Or, the task could be a collection of all the smaller tasks the receptor might be asked to perform within a given time period.

The former isolated dose prediction might be used for ALARA determination regarding receptor entry. Personnel or equipment would not be allowed to enter unless their allowable dose is greater than the predicted dose times some safety factor. The latter case, by making predictions for a given

time period, allows for determination of manloading requirements based on allowable worker dose for a given period. With regard to robotic equipment, it allows for the scheduling of equipment maintenance and down time corresponding to some time period such as daily, weekly, etc.

Cumulative dose predictions are linked to the real-time simulation of the receptor and virtual environment. Data used to form the duty cycle and accumulate dose comes directly from the user's command of the receptor via the graphical user interface. The IGRIP simulation software is programmed to update the VRF code every time the receptor moves a set distance away from its previous location or after a given amount of time has elapsed. The dose rate is updated for each location as the receptor moves in this discrete, step-wise fashion. By counting the time elapsed between calls, the VRF code is able to calculate the dose accumulated in that time interval and track the receptor's cumulative dose up to the present.

Because it may be desirable to simulate some processes at faster or slower rates, a warp factor was introduced to scale the time counted by the computer. For real-time simulation where the user is "driving" the receptor, the warp factor is set to one. For faster than real time, the warp factor is greater than unity, while the opposite is true for slower-than-real-time simulations.

The necessity for the VRF code to update the local dose rate to the receptor in real time proved to be too great a task due to the time required to recalculate the local dose rate. This was true despite the simplifications implemented with the ray analysis technique. While the computational lag time was still small and adequate for shielding and ALARA studies, it could not be adapted to real-time simulation.

Therefore, a method of prior 3D dose mapping was implemented with VRF able to look up dose rates from these previously calculated dose maps. A simple 3D dose map with comments is shown in Figure 3-2. The time involved in a multidimensional database look up scheme is negligible and allows for the real-time simulation of a receptor's duty cycle.

The first step in this process involves the generation of the 3D dose map. This was straight forward as it utilizes the previous methods for calculating local dose rates in the virtual environment. However, the additional work involves selection of the discrete 3D locations according to some user defined mesh spacing. This is done automatically by the VRF program, which prompts the user for the desired number of mesh points in each direction (x, y, and z). Also the data had to be stored in a format that could later be read by the VRF program for dose rate look up.

A shortcoming of this simple 3D dose map is that the modeled radiation environment is then static, which is not

realistic or useful for some simulations. For this reason, the ability was added for the program to generate a four-dimensional dose map, where the fourth variable could represent time or some other parameter closely associated with the simulation. For example, in simulations of Tank C-106, the fourth variable represented the waste level in the tank. This permitted predictions of the dose throughout the waste removal process as well as variable waste removal rates.

The other step involved code development to allow for look up and interpolation of the dose map data. The interpolation method allows for linear or log interpolation based on the dose ranges encountered. For simulations where the fourth variable is something other than the simulation time, a parameter must link that variable to the simulation time. This parameter can be variable and changed by the user throughout the simulation. In the example of the waste tank, the parameter linking the four-dimensional dose map and the simulation time is the cleanup rate (the rate at which the waste level is changing). This allows the cleanup rate to change during the simulation and even become zero when the cleanup equipment is not active.

Table 3-1. VRF virtual-object geometry types. Number is used to identify the type in the geometry database. Abbreviation is used by the VRF program to identify the geometry of functions that perform shielding and dose calculations. The dimension data is used to identify the parameter that is stored in a particular dimension field (variable).

Geometrical Type	Abbrev.†	Num.	Dimension 1	2	3
point	pt	0	-	-	-
line	line	1	L	-	-
disk	disk	2	R	-	-
disk, hollow	dskh	3	R_1	R_2	-
ring	ring	4	R	-	-
cylinder	cylv	5	R	H	-
cylinder, hollow	cylh	6	R_1	R_2	H
annulus, thin-walled	tann	7	R	H	t
plane	plan	8	L	W	-
box	boxv	9	L	W	H
box, hollow	boxs	10	L	W	H
sphere	sphv	11	R	-	-
sphere, hollow	sphh	12	R_1	R_2	-

† For example, cylv_dose.c is the function that calculates the dose rate from a cylindrical volume source, while sh_disk.c calculates attenuation for a disk shield.

Table 3-2. Summary of VRF input parameters.

Parameter	Symbol	Units
activity†	A	μCi
activity concentration†, volume source	A_v	$\mu Ci \cdot g^{-1}$
activity concentration†, line source	A_l	$\mu Ci \cdot cm^{-1}$
activity concentration†, area source	A_a	$\mu Ci \cdot cm^{-2}$
intensity‡	f	photons per decay
energy	E	MeV
mass attenuation coefficient	μ/ρ	$cm^2 \cdot g^{-1}$
density	ρ	$g \cdot cm^{-3}$
Berger buildup parameter α	α	unitless
Berger buildup parameter β	β	unitless
exposure dose rate	X	$R \cdot hr^{-1}$
exposure dose conversion factor	k	$R \cdot hr^{-1}$ per MeV $cm^{-2} \cdot sec^{-1}$
material dose conversion factor	--	rad-material per R
dose equivalent conversion factor	--	rem per R
volume	V	cm^3
radius	R	cm
length	L	cm
width	W	cm
height	H	cm
thickness	t	cm
relative error, allowable	-	unitless
normal value, confidence level	$Z_{\alpha/2}$	unitless

† total activity for the source
‡ photons per decay based on total source activity

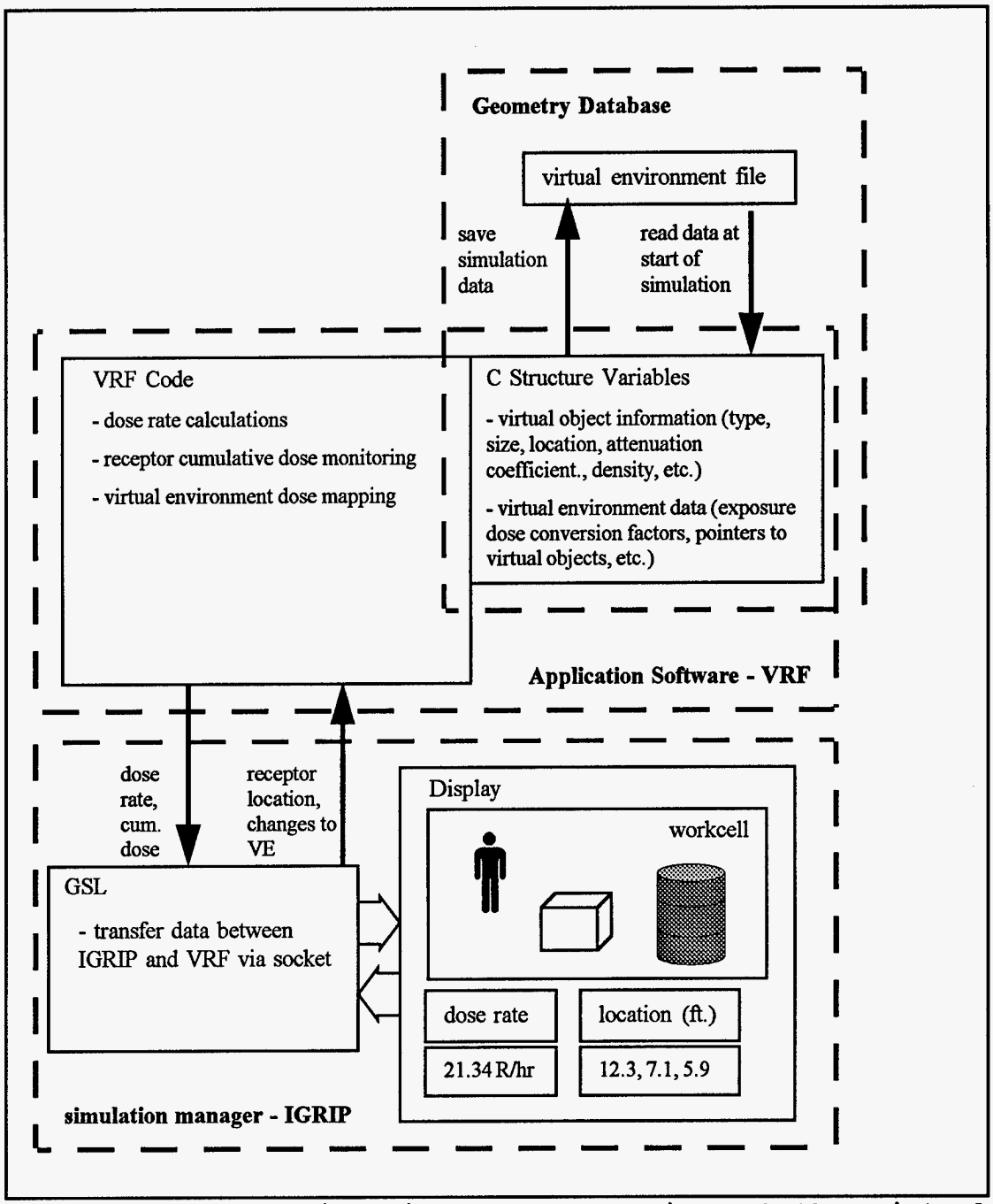

Figure 3-1. A pictorial representation of the virtual dosimeter. Dotted lines enclose the three major components with subcomponents shown as solid boxes. Arrows indicate data streams for information exchange and update.

```
C   test1.dm
C
C     simple dose map for testing functions
C
C     date of creation: 7/05/95
C
C

     3           number of dimension mapped

     0      0    linear interpolation of x & F(x)
     0      0    linear interpolation of y & F(y)
     0      0    linear interpolation of z & F(z)

            3    number of mesh points along x axis
            3    number of mesh points along y axis
            3    number of mesh points along z axis

  -1.143e+03    0.000e+00    1.143e+03     x mesh points
  -1.143e+03    0.000e+00    1.143e+03     y mesh points
   1.000e+01    5.100e+02    1.010e+03     z mesh points

C  dose rate data:
C
C  x varies across columns, constant in each row
C  y varies by row, constant in each column

C z=1.000e+01:
    8.799e+00    2.493e+01    1.168e+01
    1.124e+01    2.296e+01    1.217e+01
    1.448e+01    2.173e+01    1.254e+01

C z=5.100e+02:
    8.072e+00    1.519e+01    8.026e+00
    6.371e+00    1.357e+01    7.248e+00
    7.501e+00    1.677e+01    6.869e+00

C z=1.010e+03:
    4.942e+00    9.622e+00    4.082e+00
    5.103e+00    8.545e+00    4.829e+00
    4.792e+00    7.773e+00    4.574e+00
```

Figure 3-2. Sample dose map with explanations of the contents. Comments can be added to data files used by VRF provided: 1) a comment line begins with no numbers 2) comments appearing on the same line as data must be at the end.

CHAPTER 4
RESULTS AND DISCUSSION

Analytical Comparisons and Verification of Code

Throughout the development of the VRF code, numerous checks and comparison were made to ensure its accuracy and to eliminate any programming "bugs". Most of the work centered on the functions that calculate dose or shield attenuation. These functions were particularly prone to geometry errors since it is some times difficult to visualize the three-dimensional interplay of the various virtual objects. For example, to calculate the photon escape distance from a solid object, it is necessary to know through which face of the object it exits. These algorithms are prone to sign errors and to errors in selecting the proper escape distance when a quadratic solution is involved.

Care must be taken to ensure that the geometric algorithms give the correct answer regardless of the receptor's position. For equal distances above or below a source, the code should return the same dose to within the specified error limit. To verify the VRF code against such errors, test cases were run to check the dose levels at equal distances above and below the sources. Inconsistent answers

were a signal that something was wrong and made it possible to eliminate these bugs.

Other problems were more obvious such as possible divisions by zeros or bad programming that lead to infinite or undefined results. Some cases required checks to be coded into the program in order to prevent these errors from occurring. A lower divisor limit was established using the C define statement so that it could be easily changed should the code be used on a different platform.

Finally, to test the overall accuracy and reliability of the VRF code, comparisons were made with analytical solutions to certain problems. Figure 4-1 shows a comparison between the VRF and analytical solutions for the problem of a thin disk-like source. The two solutions compare very well as the graph shows for various heights above the source. Lower predictions by VRF can be attributed to the attenuation by the disk. The simple analytical solution does not account for this since it would involve a numerical solution and the present comparison is adequate. The difference between the two curves becomes smaller for greater distances. This can be explained by the fact that the difference attributed to attenuation is almost constant with height. So as the magnitude of the solution becomes smaller due to the geometric spreading with increased height, the difference between the solutions also becomes smaller in magnitude (error is a constant ~5% of the calculated value).

Figure 4-2 shows yet another analytical comparison this time for a thin-walled annular source. While only non-reentrant sources were applied in these simulations, the thin-walled annulus could be treated as a non-reentrant source if the receptor was confined to regions inside the annulus or directly above or below its cylindrical volume. Indeed, this exact case was necessary in the virtual waste-tank environments that are described in the following section. For these simulations, the virtual environment was defined as the cylindrical volume inside the tank. The thin annular source represented the contamination left behind on the walls as cleanup progressed. As seen from Figure 4-2, the two solutions compare nicely. Wobbly variation in the VRF solution is due to the statistical fluctuation inherent in the calculational method and lies within the specified relative error limit (±1%).

Real World Model--Tank C-106

To demonstrate the usefulness of the virtual dosimeter, a radioactive waste tank was modeled for simulating radiation doses to robotic equipment inside the tank (see Figure 1-1). The model is based on tank C-106, one of the 177 underground tanks at the Hanford reservation in Richland, Washington. Tank C-106 is one of 149 of these tanks that have a single shell consisting of carbon-steel and lining an outer wall and bottom of reinforced concrete. [Wal93, Nuc93]. Dose

predictions inside the tank are particularly useful since it has been proposed to use robotic equipment for the removal of the waste [Har93c, Har93d, Wal93]. Waste removal is necessitated by concern about the possible leakage of approximately 750,000 gallons (2.84E+6 liters) of liquid waste from 67 of the single shell tanks [Nuc93]. Under the Hanford Federal Facility Agreement and Consent Order (a Tri-Party Agreement between DOE, EPA, and Washington State Department of Ecology), the DOE is to dispose of this waste and cleanup the site.

To model the tank's radiation environment, information had to be gathered regarding its dimensions and the makeup of the waste. The tank itself is quite large with a diameter of 75 feet (2286 cm) and a height for waste disposal of 16 ft (488 cm). Waste depth in the tank is known to be 6 ft. (182.9 cm). However, this waste is not homogeneous, consisting mostly of sludge (consistency of peanut butter) and a harder sludge "heel" in the form of a solid saltcake.

Limited data exists for characterizing the distribution of the different waste forms. Available data comes from a single core sample. Variations in composition can be expected at different locations and with waste depth [Wal93]. For the purposes of this study, it was assumed that the waste had a uniform distribution throughout its volume with a density of 1.43 $g \cdot cm^{-3}$. Furthermore, to facilitate comparison with the previously reported values, the assumption of 44 $\mu Ci \cdot g^{-1}$ (1.63

MBq·g^{-1}) of ^{137}Cs in equilibrium with ^{137m}Ba was adopted. Since ^{137}Cs (^{137m}Ba) was the main contributor to the dose in previous studies (about 95%), it was adopted as the single radionuclide to be modeled. The other 5% was due to bremsstrahlung produced through the decay of ^{90}Sr.

The input values for the relevant VRF parameters are summarized in Table 4-1. To obtain values for parameters such as attenuation coefficients and buildup factors, assumptions had to be made about the waste's elemental composition. Previous sensitivity studies have shown the dose rates to be "extremely insensitive to changes in composition provided the density of the material does not change" [Wal93, p. E-13]. Therefore, based on the availability of buildup factor data, a composition of water, aluminum, and iron was assumed with weight percentages of 50%, 33%, and 17% respectively. Previous studies had also included sodium among the aluminum and iron in unspecified proportions.

Based on the data and assumptions, it was possible to predict the dose at any point inside the tank. To compare with reported values, the dose rate was calculated by VRF at the center, top of the tank's dome. The reported value was 14.04 R·hr^{-1} (1.007E-6 C·kg^{-1}·s^{-1}), while VRF predicted a value of 14.11 R·hr^{-1} (1.012E-6 C·kg^{-1}·s^{-1}). While the difference is only 0.5%, the VRF prediction is probably high by about 6% since the bremsstrahlung resulting from the decay of ^{90}Sr was not modelled. VRF's over prediction is likely due to

uncertainty in the input data and the application of infinite geometry buildup factors as discussed in Chapter 3.

In order to visualize and record the dose rate variation inside the tank, a dose rate profile was constructed at different heights. Figure 4-3 shows the radial dose rate profile for 1, 2, 4, and 6 meters above the waste surface. Dose rate begins to fall off as the receptor moves toward the tank wall where it is farthest from the bulk of the waste. Additionally, dose rate decreases as the receptor moves upward away from the waste surface and the tank subtends a smaller and smaller solid angle.

Still other profiles are possible to characterize the dose rate inside the tank. Since the objective of work inside the tank is to remove the waste, information on how dose rate varies with waste height is necessary and useful. Tank cleanup can be simulated by simply changing the waste level used in the dose rate calculation. However, some waste remains behind as contamination on tank walls and hardware since the cleanup process is not 100% effective. Therefore, to better model the dose rate, a uniform layer of contamination can be assumed to remain behind on the tank walls. Figure 4-4 presents the dose rate profiles in the tank when 99% of the waste is removed. Of the remaining 1% waste, 10% is evenly distributed as contamination on tank walls up to the original waste height in the tank. The remaining 90% forms the remainder of the hardened heel that would be

expected on the tank bottom. Here again, the dose rate decreases for increased height and distance from the tank center. However, the relative rate of decrease as the receptor moves toward the tank walls is not as great. This can be attributed to the contamination that remains behind.

From Figure 4-4 it is also clear that the dose rate dose not decrease proportional to the amount of waste removed. Originally, with all the waste present, the centerline dose rate at 1 meter was about 27 $R \cdot hr^{-1}$, while with 99% of the waste removed, the dose rate has fallen to a mere 5.5 $R \cdot hr^{-1}$. This disproportionality would remain even if the contamination on the walls was neglected. Instead, this effect can be attributed to self-shielding by the source material. As Figure 4-5 illustrates, the dose rate remains nearly constant for a fixed height above the waste surface as the waste is removed. Until the waste level falls below ~35 cm, no appreciable change in the dose rate is observed. In Figures 4-3 through 4-5, note that the dose rate is given relative to the waste surface, since this would be the working height of any equipment introduced to the tank.

The results presented so far, while revealing, do not take advantage of the virtual dosimeters ability to simulate processes. The cleanup process is a four-dimensional (4D) problem of space and time. Dose rate varies with location in the tank as well as with the time since initiation of cleanup operations. To simulate the dose received by a receptor

during waste removal, a 4D dose map was generated with 147 points arranged in a 3D grid (x, y, and z) and calculated for nine different waste levels in the tank ranging from 100% to 1% of the original waste height.

Using this 4D dose map, the dose rate at any location and time can be obtained by interpolation. Cleanup rate is the link between simulation time and waste level, which is how the dose map is tabulated. This allows for a variable cleanup rate as well as dose accumulation when the equipment is idle (cleanup rate is zero). Several simulations were examined with different cleanup periods (days required to complete waste removal), effective hours of operation per day, and cleanup rate. Since there is a fixed initial amount of waste, the average cleanup rate during operation is also fixed for a given cleanup period and daily effective hours of operation.

Results of these simulations are summarized in Table 4-2. Obviously, the lowest total cumulative dose is achieved for the shortest cleanup periods. Also, for the same cleanup period, the total dose is lower for shorter effective hours of operation per day. This is true because when the equipment is not in operation it is assumed to be positioned in the upper part of the tank where the dose rate is lower. When operating, the equipment is down near the waste surface where the dose rate is higher. Regardless, for the same effective hours of operation per day, the total dose is approximately linear with cleanup period. Therefore, to minimize the does

received during waste removal, the cleanup period should be shortened as much as possible. The effective hours of operation is not as important provided the necessary cleanup rate can be achieved for the desired cleanup period.

However, the above observations change if the equipment is shielded during idle periods. For a significant dose rate reduction by shielding, the cleanup period can be greatly extended if necessary. The limiting factor then becomes cleanup rate since this determines the total operating time and the total time spent in the high dose areas near the waste surface. For a dose reduction factor of 4.5, which can be achieved with 1 cm of lead or lead equivalent, reductions in total cumulative dose as high as 39% can be achieved (see Table 4-2). The dose reduction allows for a longer stay time in the tank should it become necessary. Ordinarily, it would not be desirable to extend the cleanup period. However, this would be important if the equipment had to be idled occasionally to perform tank inspections, checking for possible leaks or assaults on the tank's integrity.

VRF Shielding Studies

The VRF program can be used to evaluate the effectiveness of various shields at reducing dose rate levels to receptors. Shields of different size, thickness, and materials can be created and positioned at any location in the 3D virtual environment. For example, a lead shield with radius of 50 cm

and thickness 1 cm reduces the dose rate at the tank's center dome from 14.11 $R \cdot hr^{-1}$ to 3.14 $R \cdot hr^{-1}$. The virtual shield is placed 10 cm below the virtual receptor point since a real receptor has a finite size and would not receive the full protection of the shield.

Figure 4-6 shows the dose rate profile across the face of a disk shield made of lead. It has a radius of 30 cm, a thickness of 1 cm and is located at the half radius of tank C-106. Its height is 390 cm with dose rate calculated at 400 cm (10 cm above the shield). The graph in Figure 4-6 shows the dose rate to be depressed across the disk and immediate surrounding area. At its center the dose rate is reduced from 18.9 $R \cdot hr^{-1}$ (unshielded) to 4.05 $R \cdot hr^{-1}$ (shielded).

However, the lowest dose rate is not found at the shields center but at a radius of 15 cm on the side nearest the tank wall. Indeed, the entire dose rate profile appears skewed in that direction. This is due to the shield being located at the half radius of the source. Locations over the shield nearest the tank center do not receive as much protection as points located 180° opposite nearest the tank wall. The radial off set from tank center allows the receptor to "see" more of the source material on the side nearest the tank center.

Also, from Figure 4-6, the effective area of the shield can be seen to have a diameter of about 30 cm. The outer 10 to 20 cm of the shield experiences a rapid increase in the

dose rate as the receptor moves toward the shield's edge. This information would be useful in shielding design. An extra 10 to 20 cm should be added to the radius of the area to be shielded. In addition, for shielding locations off source centerline, receptors should use the side farthest from the source centerline to utilize the more effective parts of the shield.

Similar results are obtained for a shield of radius 50 cm as shown in Figure 4-7. Here the effective area of the shield is larger with a diameter of about 70 cm. Again the 10 to 20 cm edge of the shield experiences a rapid increase in dose rate. Also, the profile shows the characteristic skewed behavior for a location off set from the source centerline.

Table 4-1. Summary of VRF input parameters for tank C-106 model with their corresponding values.

Parameter	Value	Units
activity, volume source	44	$\mu Ci \cdot g^{-1}$
number of source photon energies†	1	--
intensity†	0.901	photons per decay
energy†	0.6617	MeV
mass attenuation coefficient (0.5 MeV)‡	0.090	$cm^2 \cdot g^{-1}$
mass attenuation coefficient (1.0 MeV)‡	0.066	$cm^2 \cdot g^{-1}$
density	1.43	$g \cdot cm^{-3}$
Berger buildup parameter α (0.5 MeV)‡	1.573	unitless
Berger buildup parameter α (1.0 MeV)‡	1.096	unitless
Berger buildup parameter β (0.5 MeV)‡	0.104	unitless
Berger buildup parameter β (1.0 MeV)‡	0.057	unitless
exposure dose conv. factor (0.6 MeV)	1.94E-6	$R \cdot hr^{-1}$ per MeV $cm^{-2} \cdot sec^{-1}$
exposure dose conv. factor (0.7 MeV)	1.92E-6	$R \cdot hr^{-1}$ per MeV $cm^{-2} \cdot sec^{-1}$
radius	1143	cm
height	182.9	cm

† ^{137}Cs is assumed to be the major contributor to the radiation dose inside the tank [Wal93]. Energy and intensity data for ^{137}Cs was taken from NCRP 58, 1985.

‡ These are composite values for the sludge/saltcake material based on the assumption of 50% H_2O, 33% Al, and 17% Fe (all weight percent). Attenuation data was taken from Foderaro, 1978 and buildup data from Schaeffer, 1973.

Table 4-2. Summary of total cumulative dose predictions for tank C-106 cleanup operations.

Cleanup Period (days)	Effective Hours of Operation (hours/day)	Cleanup Rate (m^3/hour)	Total Cumulative Dose (Roentgen)	(rad-SiO_2)
unshielded:				
15	10	5.00	7.96E+3	6.98E+3
15	20	2.50	9.16E+3	8.04E+3
30	10	2.50	1.63E+4	1.43E+4
30	20	1.25	1.91E+4	1.67E+4
90	10	0.83	4.91E+4	4.31E+4
90	20	0.42	5.47E+4	4.80E+4
shielded:†				
15	10	5.00	5.06E+3	4.44E+3
15	20	2.50	8.12E+3	7.12E+3
30	10	2.50	1.00E+4	8.77E+3
30	20	1.25	1.75E+4	1.53E+4
90	10	0.83	3.04E+4	2.67E+4
90	20	0.42	4.82E+4	4.23E+4

† The equipment was shielded when idle at its storage point 400 cm above the waste. A lead shield of radius 50 cm and thickness 1 cm was used for shielding the equipment.

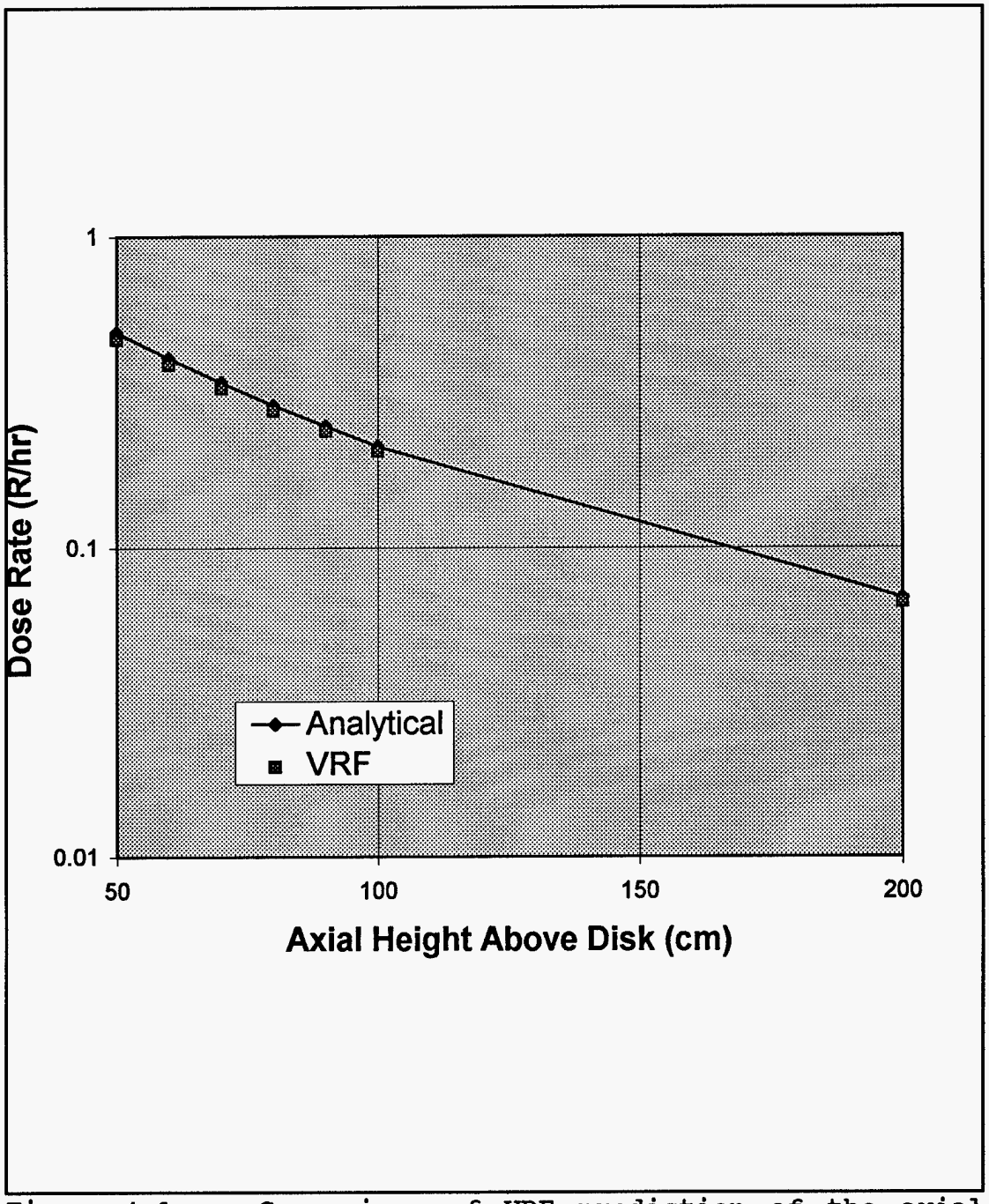

Figure 4-1. Comparison of VRF prediction of the axial centerline dose rate profile with the analytical solution for a thin disk source.

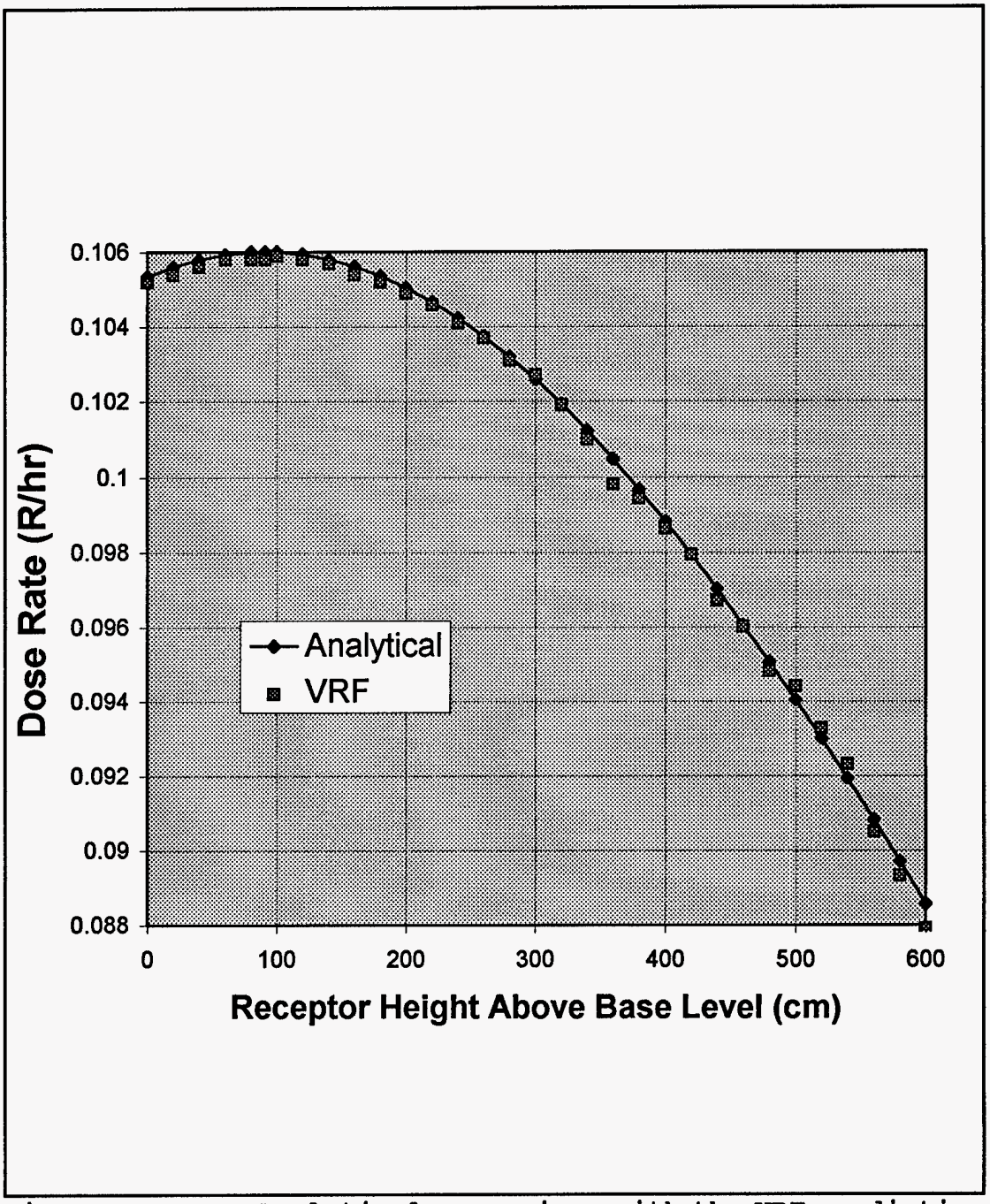

Figure 4-2. Analytical comparison with the VRF prediction of the axial centerline dose rate profile for a thin-walled annular source. The source height extends from 0 to 181.3 cm above base level.

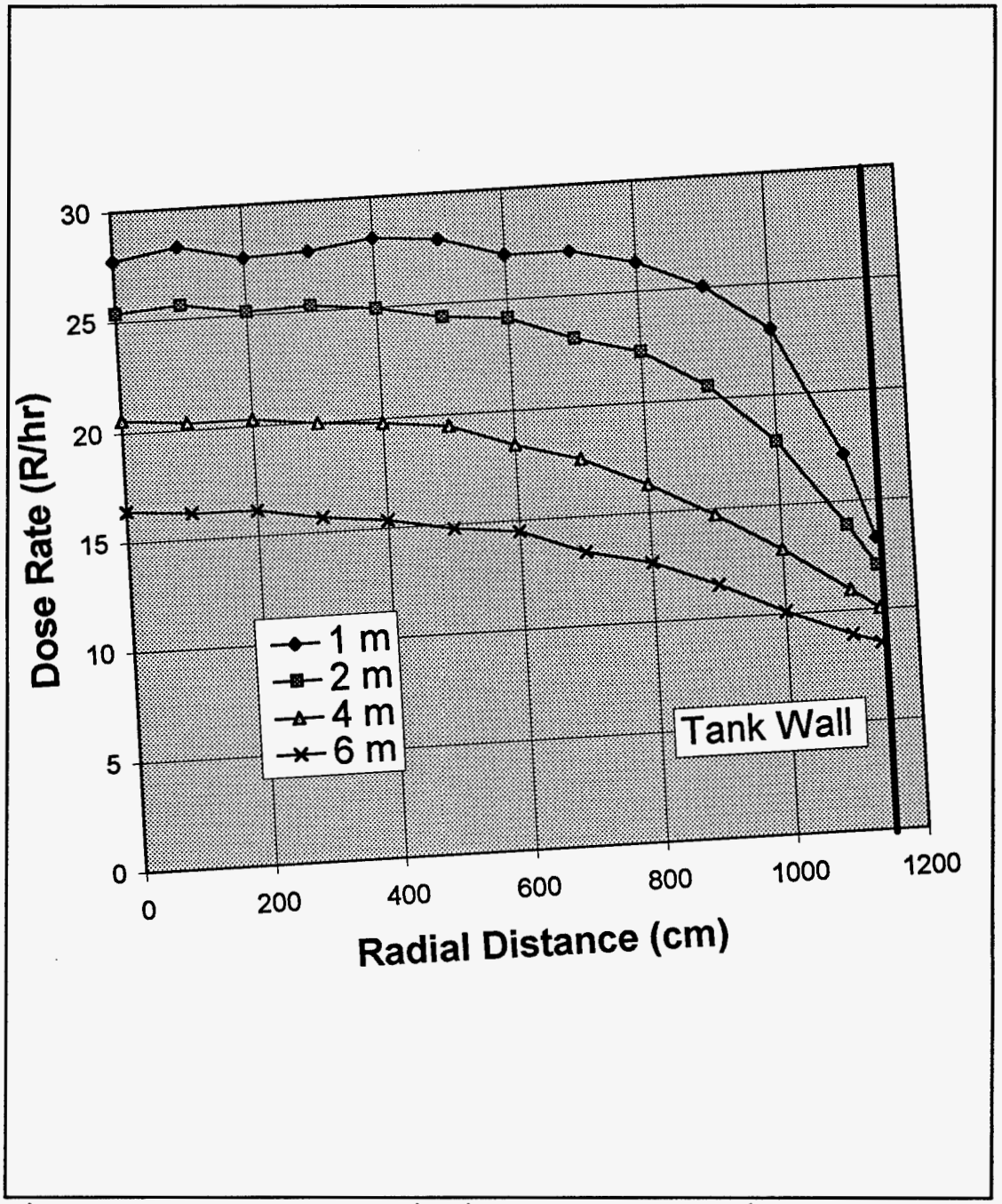

Figure 4-3. VRF prediction of the radial dose rate profile of tank C-106 at four different heights above the waste surface. Waste height in the tank equals 183 cm.

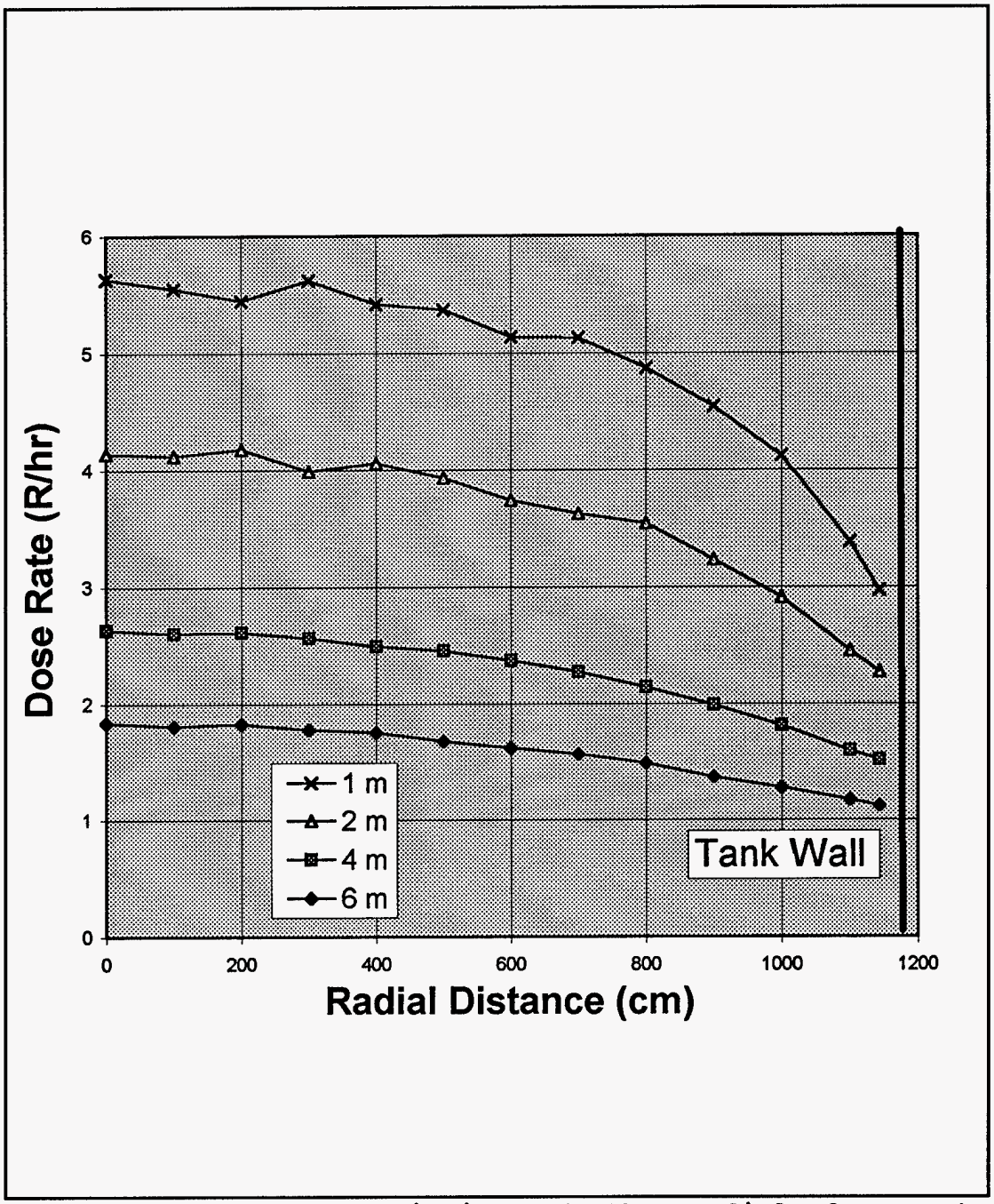

Figure 4-4. VRF prediction of the radial dose rate profile of tank C-106 with 99% of the waste removed. Of the remaining waste, 10% is assumed to be contamination on the tank walls with the rest forming a uniform heel at the bottom of the tank.

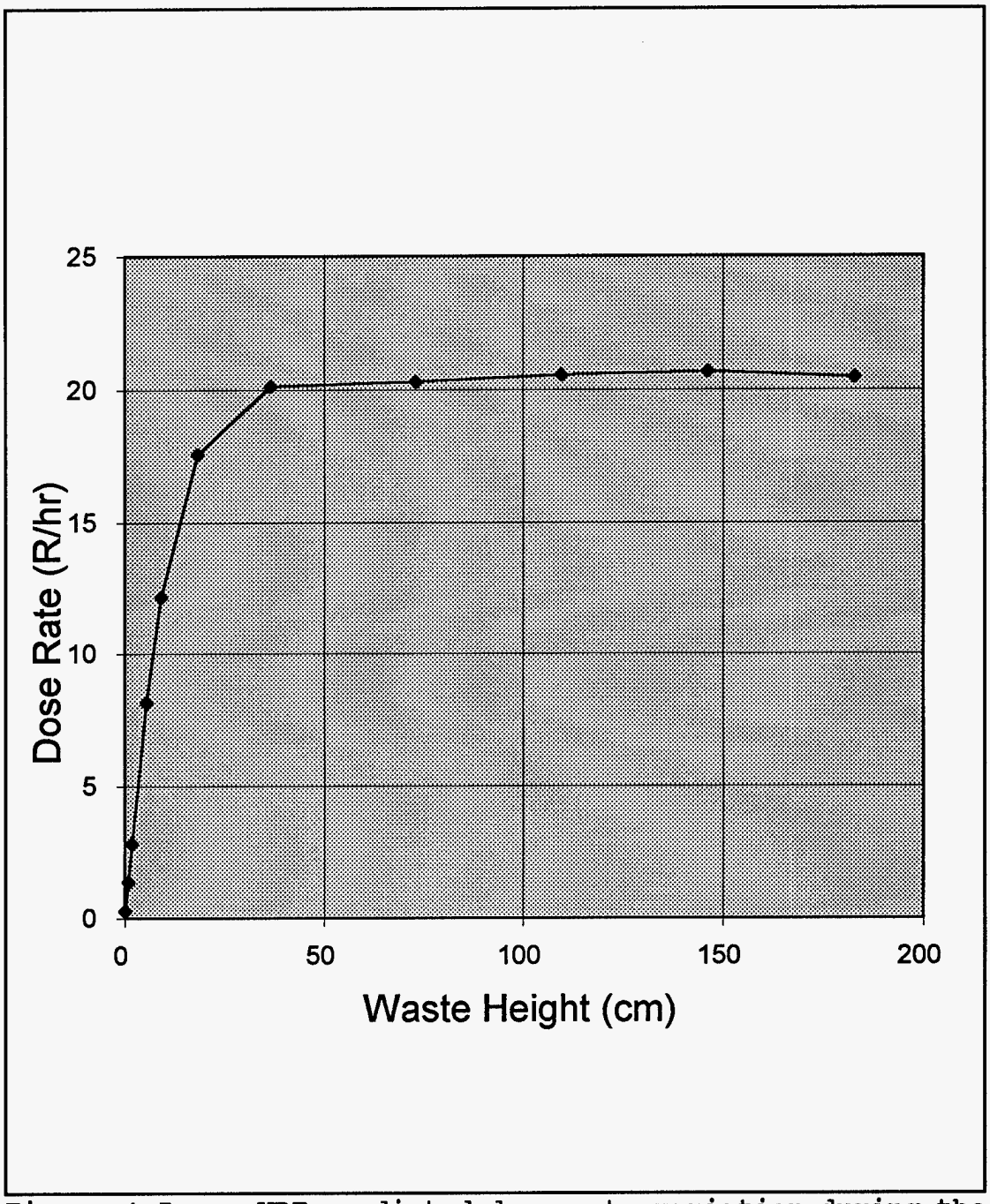

Figure 4-5. VRF predicted dose rate variation during the waste removal process. The dose rate is for a constant receptor height of 400 cm above the waste surface.

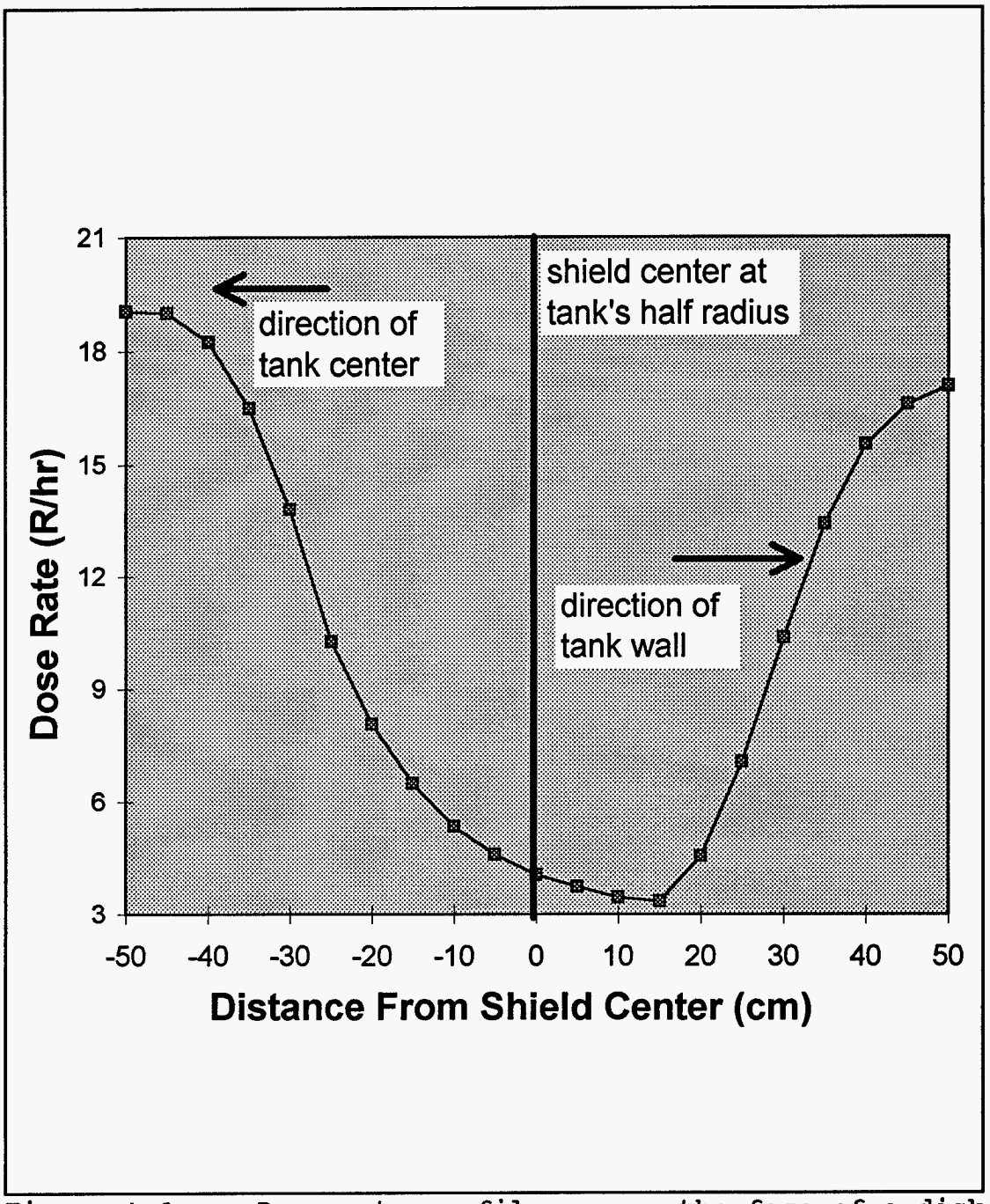

Figure 4-6. Dose rate profile across the face of a disk shield (30 cm radius, 1 cm thick, lead). The shield is centered at the half-radius of tank C-106 at a height of 390 cm. Dose rate is calculated at 10 cm above the shield.

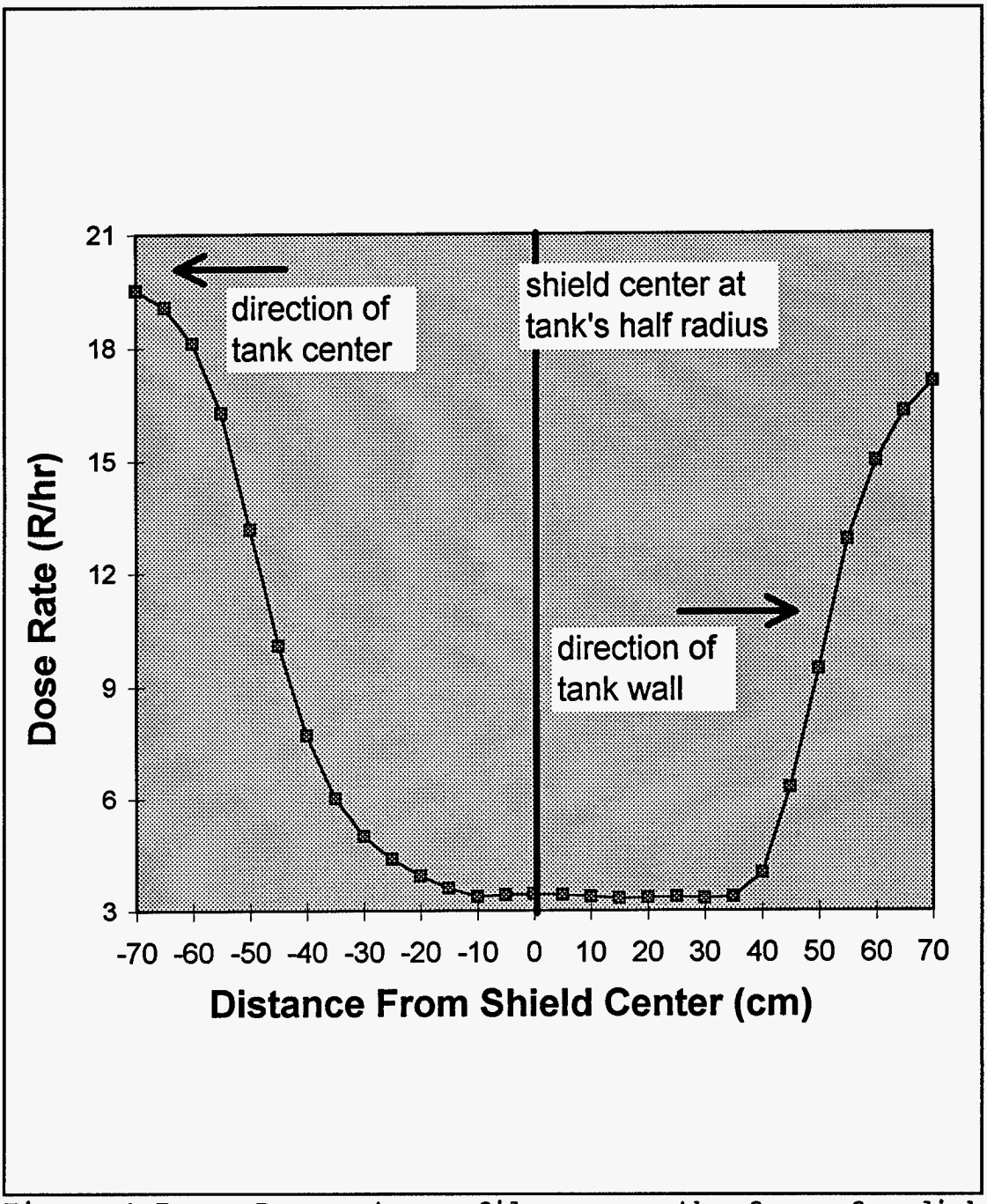

Figure 4-7. Dose rate profile across the face of a disk shield (50 cm radius, 1 cm thick, lead). The shield is centered at the half-radius of tank C-106 at a height of 390 cm. Dose rate is calculated at 10 cm above the shield.

CHAPTER 5
CONCLUSIONS

Advances in computer technology are making possible the concept of virtual engineering for the designing, planning, and testing of projects in the virtual world. Most significantly, this study demonstrates the usefulness of a virtual dosimeter as another facet for consideration in any virtually engineered project where radiation is involved. The construction of an underlying computer model of a radiation environment is not new or different. However, the added immersion associated with its 3D display and the interactive nature of a graphical user interface brings ALARA considerations in to a new environment.

The VRF program developed in this work allows for ALARA considerations in multiple source, multiple object environments with no restrictions on their arrangement. However, making it broad in scope forced certain assumptions with regard to the physical processes that could be modeled. These limitations are owing to the chief tenants of any virtual system--namely, immersion and interaction. To maintain the speed of the simulation's update, a ray analysis method had to be adopted with empirically derived corrections for radiation buildup. Despite the assumptions and

limitations necessary for its development, this work lays a wide foundation for the addition of other virtual object geometries, dosimetric capabilities, and innovations in graphical display.

The application environment modeled in this study, tank C-106, illustrates how virtual dosimetry is applied to ALARA determinations. By simulating the receptor's duty cycle, VRF can make accurate predictions of total cumulative dose. It also facilitates the comparison of various shielding scenarios at different stages in the duty cycle. As an example, simulation analysis of the receptor's tank-cleanup duty cycle revealed a possible dose reduction of 39% by simply shielding the receptor during idle periods. Utilization of the VRF program can provide additional insights for the development of an effective ALARA program.

REFERENCES

Ang94 G. ANGELINI, K. FAST, and D. WILLIAMS, "IGRIP as A Unified Virtual Environment for Simulation Based Design," Proceedings of the 1994 Deneb IGRIP User's Conference, 59 (1994)

Att86 F. H. ATTIX, Introduction to Radiological Physics and Radiation Dosimetry, John Wiley and Sons, New York, NY (1986)

Bog93 W. BOGUS and R. RACZYNSKI, "Calculation of Dose and Dose-rate Distribution for Gamma-Irradiated Materials," Radiat. Phys. Chem., **42**, 4-6, 773 (1993)

Bra92 M. BRAIN, MOTIF Programming, The Essentials ... and More, Digital Press, Burlington, MA (1992)

Cem83 H. CEMBER, Introduction to Health Physics, McGraw-Hill, New York, NY (1983)

Chi84 A. B. CHILTON, J. K. SHULTIS, and R. E. FAW, Principles of Radiation Shielding, Prentice-Hall, Englewood Cliffs, NJ (1984)

Cra90a C. D. CRANE and J. S. TULENKO, "An Advanced Semiautonomous Robotic System for Hazardous Response Work for Decontamination and Decommissioning," Trans. Am. Nucl. Soc., **62**, 601 (1990)

Cra90b C. D. CRANE III, G. R. DALTON, J. OGLES, J. S. TULENKO, and X. ZHOU, "Faster-Than-Real-Time Robot Simulation for Plan Development and Robot Safety," Trans. Am. Nucl. Soc., **61**, 408 (1990)

Dal90 G. R. DALTON, J. S. TULENKO, and X. ZHOU, "Concurrent Use of Data Base and Graphics Computer Workstations to Provide Graphic Access to Large, Complex Data Bases for Robotics Control of Nuclear Surveillance and Maintenance," Trans. Am. Nucl. Soc., **61**, 407 (1990)

Dal91 G. R. DALTON, J. S. TULENKO, H. DAI, and S. CLIFFORD, "Use of Three-Dimensional Graphics Modeling in Nuclear Design," Trans. Am. Nucl. Soc., **64**, 628 (1991)

Dur95 N. I. DURLACH and A. S. MAVOR, Virtual Reality, Scientific and Technological Challenges, National Academy Press, Washington, D.C. (1995)

Egg94 D. EGGLESTON, "So, What's Virtual Reality Good for Anyway?" Proceedings of the 1994 Deneb IGRIP User's Conference, 51 (1994)

Ekd91 D. EKDAHL, J. S. TULENKO, L. UTLEY, and H. HAMILTON, "On-Line Annealing Processes for Hardening Electronic Components in Mobile Robots for Radiation Environments," Trans. Am. Nucl. Soc., **64**, 616 (1991)

Fod78 A. FODERARO, The Photon Shielding Manual, Pennsylvania State University, Department of Nuclear Engineering, University Park, PA (1978)

Gla95 W. A. GLAUSER, "How Computational Chemistry Techniques Can Be Applied in Biotechnology: An Overview," Scientific Computing and Automation, **12**, 9, 23 (1995)

Had94 D. HADDOX, S. CLIFFORD, D. EKDAHL, and J. S. TULENKO, "Virtual Reality for Mobile Robot Control," Proceedings of the 1994 Deneb IGRIP User's Conference, 91 (1994)

Har93a Y. HARIMA "An Historical Review and Current Status of Buildup Factor Calculations and Applications," Radiat. Phys. Chem., **41**, 4-5, 631 (1993)

Har93b Y. HARIMA and H. HIRAYAMA, "Detailed Behavior of Exposure Buildup Factor In Stratified Shields for Plane-Normal and Point Isotropic Sources, Including the Effects of Bremsstrahlung and Fluorescent Radiation," Nuclear Science and Engineering, **113**, 367 (1993)

Har93c R. W. HARRIGAN, "Automating the Operation of Robots in Hazardous Environments," Proceedings of the 1993 IEEE/RSJ International Conference on Intelligent Robots and Systems, 1211 (1993)

Har93d R. W. HARRIGAN, "Automating the Control of Robotic Systems In Unstructured Environments," Proceedings of the 1993 International Symposium On Intelligent Control, 81 (1993)

Hin90 D. E. HINTENLANG, J. S. TULENKO, R. WHEELER, and T. ROY, "Environmental Hardening of Robots for Nuclear Maintenance and Surveillance Tasks," Trans. Am. Nucl. Soc., **61**, 410 (1990)

Ill94 D. L. ILLMAN, "Researchers Make Progress in Applying Virtual Reality to Chemistry," Chemistry and Engineering News, **72**, 22 (1994)

Jae68 R. G. JAEGER, E. P. BLIZARD, A. B. CHILTON, and m. GROTHENHUIS, Engineering Compendium on Radiation Shielding Volume I: Shielding Fundamentals and Methods, Springer Verlag, New York, NY (1968)

Jon95 S. JONES and J. S. TULENKO, "ANDROS gets ready for the hot jobs," Nuclear Engineering International, **40**, 487, 28 (1995)

McI90 R. MCINTYRE, C. J. HUNTZINGER, and W. R. NELSON, "Application of EGS4 to Industrial Irradiator Design and Use," Radiat. Phys. Chem., 35, 4-6, 762 (1990)

Mic88 Microshield 3.13, Grove Engineering, Inc., Rockville, MD (1988)

Mur94 R. L. MURRAY, Understanding Radioactive Waste, Battelle Press, Columbus, OH (1994)

NCR76 NCRP Report No. 49--Structural Shielding Design and Evaluation for Medical Use of X Rays and Gamma Rays of Energies Up to 10 Mev, National Council on Radiation Protection and Measurements, Bethesda, MD (1976)

NCR85 NCRP Report No. 58--A Handbook of Radioactivity Measurements Procedures, National Council on Radiation Protection and Measurements, Bethesda, MD (1985)

Nuc93 The Nuclear Waste Primer, League of Women Voters Education Fund, Washington, DC (1993)

Pim93 K. PIMENTEL and K. TEIXEIRA, Virtual Reality--Through the New Looking Glass, Intel/Windcrest/McGraw-Hill, New York, NY (1993)

Pre94 J. PREECE, Y. ROGERS, H. SHARP, D. BENYON, S. HOLLAND, and T. CAREY, Human-Computer Interaction, Addison-Wesley Publishing Company, Workingham, England (1994)

Rai90 G. R. RAISALI, M. SOHRABPOUR, and A. HADJINIA, "A Computer Code for Dose Rate Mapping of Gamma Irradiators," Radiat. Phys. Chem., **35**, 4-6, 831 (1990)

Rai93 G. R. RAISALI and M. SOHRABPOUR, "Application of EGS4 Computer Code for Determination of Gamma Ray Spectrum and Dose Rate Distribution in Gammacell 220," Radiat. Phys. Chem., **42**, 4-6, 799 (1993)

Sad94 J. SADOWSKY and R. W. MASSOF, "Sensory Engineering: The Science of Synthetic Environments," Johns Hopkins APL Technical Digest, **15**, 2, 99 (1994)

Sch73 N. M. SCHAEFFER, Reactor Shielding for Nuclear Engineers (TID-2595), U. S. Atomic Energy Commission, Office of Information Services, Springfield, VA (1973)

Sch92 B. SCHLEIEN, The Health Physics and Radiological Health Handbook, Scinta Inc., Silver Spring, MD (1992)

Sch95 R. J. SCHWARTZ, "Virtual Facilities: Imaging the Flow," Aerospace America, **33**, 7, 22 (1995)

Shr66 Y. A. SHREIDER, The Monte Carlo Method, Pergamon Press, Long Island City, NY (1966)

Sin91 M. K. SINHA and S. K. KULKARNI, "Computer Code for Dose-distribution in a Multi-element Gamma Irradiation Cell," Appl. Radiat. Isot., **42**, 1, 41 (1991)

Tau94 G. TAUBES, "Taking the Data in Hand-Literally-With Virtual Reality," Science, **265** 884, (1994)

Vir95 "Virtual Engineering Pioneers New Approach," Scientific Computing and Automation, **12**, 9, 33 (1995)

Wal93 "Project W-340 Manipulator Retrieval System for Tank 241-C-106," WHC-SD-W340-ES-001, Westinghouse Hanford Company, Hanford, WA (1993)

Woo82 J. WOOD, Computational Methods in Reactor Shielding, Pergamon Press, Elmsford, NY (1982)

APPENDIX
LISTING AND EXPLANATION OF THE VRF CODE

Listing of VRF Code Functions (Files)

Date	Time	Size bytes	Name
11/04/95	02:36p	6,731	bb_attn.c
11/04/95	02:43p	6,517	boxv_dose.c
11/04/95	02:43p	6,765	cylv_dose.c
11/04/95	02:43p	5,772	disk_dose.c
11/04/95	02:19p	2,470	doserate.c
10/07/95	05:42p	4,523	doserate_dm.c
10/20/95	01:31p	4,089	dose_dm.c
10/27/95	09:27p	3,760	igrip_serv.c
09/25/95	09:55a	2,212	int1d.c
09/24/95	11:31a	688	int1dl.c
11/04/95	02:43p	5,365	line_dose.c
10/25/95	09:26p	9,364	make_dm.c
11/04/95	02:43p	3,633	pt_dose.c
11/04/95	02:11p	4,725	pxvrfve.c
11/02/95	03:39p	5,835	pxvrf_igrip.c
11/02/95	05:21p	3,061	radata.c
10/25/95	09:26p	3,246	read_dm.c
09/25/95	09:56a	2,501	read_dms.c
11/02/95	01:57p	2,282	read_num.c
11/02/95	05:03p	6,353	read_ve.c
11/04/95	01:42p	4,645	sh_disk.c
10/24/95	06:09a	16,739	tank4d_1.dm
11/04/95	02:43p	4,663	tann_dose.c
09/25/95	09:57a	661	test1.dm
11/02/95	04:19p	2,834	vefile.dat
11/02/95	04:53p	4,500	vrftop.c
10/25/95	08:39p	3,348	write_dm.c

Description of VRF Code Functions

bb_attn.c

This function calculates the broad beam attenuation of a gamma ray between birth and the receptor including attenuation and buildup in the source material. Berger's formula for

buildup is applied to each attenuating medium. In addition, Broder's formula is applied to cases involving multiple attenuating objects.

boxv_dose.c

This function calculates the dose rate (R/hr) at the receptor point from a box (volume) source.

cylv_dose.c

This function calculates the dose rate (R/hr) at the receptor point from a cylinder (volume) source.

disk_dose.c

This function calculates the dose rate (R/hr) at the receptor point from a disk (area) source.

doserate.c

This function calculates the total dose rate (R/hr) at the receptor point for all sources currently defined in the virtual environment. It calls the appropriate functions to calculate the dose rate from each source based on its geometrical type.

doserate_dm.c

This function looks up and interpolates the local dose rate at a receptor's location using a dose map stored in memory.

dose_dm.c

This function receives updates on the receptor's position as it moves about the virtual environment (updates come from igrip_serv.c). It updates the local dose rate at each new location and monitors the total cumulative dose received. The receptor's cumulative dose is returned to igrip_serv.c so that it can be displayed in a GSL popup window.

igrip_serv.c

This function sets up a link with IGRIP to pass information between VRF and IGRIP via a socket. This function must be engaged to simulate the dose to a receptor in performance of a duty cycle. It receives the new receptor location and calls dose_dm.c to update the total cumulative dose received up to the current point.

int1d.c

This function interpolates (linear or log) for given set of numbers supplied by the calling program.

int1dl.c

This function does simple linear interpolation for a given set of numbers supplied by the calling program.

line_dose.c

This function calculates the dose rate (R/hr) at the receptor point from a line source.

make_dm.c

This function generates a dose map of the current virtual environment. It prompts the user for the number of mesh points and the name of a file for storing the dose map.

pt_dose.c

This function calculates the dose rate (R/hr) at the receptor point from a point source.

pxvrfve.c

This is the program that coordinates most of the VRF functions. It does not include IGRIP communication (using igrip_serv.c). Instead it is intended for nongraphical off-line work with VRF when the graphical simulation is not engaged.

pxvrf_igrip.c

This also is a program that coordinates most of the VRF functions including IGRIP communications used during graphical simulations.

radata.c

This function sets up a 4D array of radiological data (mass attenuation coefficient, Berger buildup parameter α and β). It interpolates these parameters for every virtual object (sources and structures) for every source energy found in the virtual environment. This data is accessed by each of the dose-rate-calculation functions when starting a new calculation. The data is looked up by the ordered object number for each ordered energy of each ordered source (see Figure A-1).

read_dm.c

This function reads in a dose map from a file. The function prompts the user for the filename. The read process is subject to the non-numeric commenting restrictions described for read_num.c.

read_dms.c

This function reads in a dose map from a file. The calling program supplies the name of the file to be read. The read process is subject to the non-numeric commenting restrictions described for read_num.c.

read_num.c

This function reads the next number (double or integer) from a file and stores it in a variable supplied by the calling program. It simply reads the next number it finds regardless (can be in scientific notation). All characters are ignored by the function. For example, a line beginning with a non-numeric will be ignored entirely and any number following a non-numeric on any given line will also be ignored.

read_ve.c

This function reads in the data for a virtual environment that is stored in a file. The function prompts the user for

the filename. The read process is subject to the non-numeric commenting restrictions described for read_num.c.

sh_disk.c

This function calculates the number of mean free paths of attenuation through a virtual object for a given gamma-ray. This information is returned to bb_attn.c for calculating the attenuation.

tank4d_1.dm

This is a sample 4D dose map of tank C-106.

tann_dose.c

This function calculates the dose rate (R/hr) at the receptor point from a cylinder (volume) source.

test1.dm

This is a sample 3D dose map with comments.

vefile.dat

This is a sample virtual environment data file.

vrftop.c

This code contains all the define statements necessary for the functions to compile and operate properly.

write_dm.c

This function writes out the current dose map to a file. It prompts the user to supply a filename.

Explanation of Dose Map Data Fields

The following is a listing of all the data fields for a dose map file. Brackets "[]" indicate an individual numerical

data field. Italicized text provides an explanation of the data field(s) that follow it. An underlined piece of text represents a countable quantity of a particular type of data and may be used later to indicate the terminating quantity of a particular type of data. For example, NG{1} represents the number of grid spaces for the first dimension (x, y, z, etc.) and the NG{1}th index represents the last piece of data counted from 1 to NG{1}. Accordingly, X{ NG{1} } represents the data point of type X for NG{1}th quantity. Dots are used to indicate the omission of part of a series of ordered data points.

number of dimensions (i.e. x, y, z, t, etc.) for the dose map, integer, up to MAXDIM.

[ND]

array designating linear or log interpolation for each independent dimension variable and the dependent variable with respect to each independent dimension variable, integers, 0 for linear and 1 for log.

[1st independent dimension variable]
[dependent variable with respect to 1st dimension variable]
. . . . . .
. . . . . .
. . . . . .
[NDth independent dimension variable]
[dependent variable with respect to Ndth dimension variable]

number of mesh (grid) points for each dimension, integers, up to MAXGRID

[NG{1}, number of points for the 1st dimension]
. . . . . .
. . . . . .
. . . . . .
[NG{ND}, number of points for the NDth dimension]

array of mesh points for each dimension, reals

[1st mesh point, 1st dimension] ... [NG{1}th mesh point]
. . . . . .
. . . . . .
. . . . . .

[1st mesh point, NDth dimension] ... [NG{ND}th mesh point]

dose rate data points, shown for up to four dimensions

at T{1}, set 1 of the 4th dimension:

at Z{1}, set 1 of the 3rd dimension:

```
[at X{1}, Y{1}] ... [at X{NG{1}}, Y{1}]
.    .    .    .    .    .    .    .    .    .
.    .    .    .    .    .    .    .    .    .
.    .    .    .    .    .    .    .    .    .
[at X{1}, Y{NG{2}] ... [at X{NG{1}}, Y{NG{2}}]
```

at Z{2}, set 2 of the 3rd dimension:

```
[at X{1}, Y{1}] ... [at X{NG{1}}, Y{1}]
.    .    .    .    .    .    .    .    .    .
.    .    .    .    .    .    .    .    .    .
.    .    .    .    .    .    .    .    .    .
[at X{1}, Y{NG{2}] ... [at X{NG{1}}, Y{NG{2}}]

.    .    .    .    .    .    .    .    .    .

.    .    .    .    .    .    .    .    .    .

.    .    .    .    .    .    .    .    .    .
```

at Z{NG{3}}, set NG{3} of the 3rd dimension:

```
[at X{1}, Y{1}] ... [at X{NG{1}}, Y{1}]
.    .    .    .    .    .    .    .    .    .
.    .    .    .    .    .    .    .    .    .
.    .    .    .    .    .    .    .    .    .
[at X{1}, Y{NG{2}] ... [at X{NG{1}}, Y{NG{2}}]
```

at T{2}, set 2 of the 4th dimension:

at Z{1}, set 1 of the 3rd dimension:

```
[at X{1}, Y{1}] ... [at X{NG{1}}, Y{1}]
.    .    .    .    .    .    .    .    .    .
.    .    .    .    .    .    .    .    .    .
.    .    .    .    .    .    .    .    .    .
[at X{1}, Y{NG{2}] ... [at X{NG{1}}, Y{NG{2}}]
```

at Z{2}, set 2 of the 3rd dimension:

```
[at X{1}, Y{1}] ... [at X{NG{1}}, Y{1}]
.    .    .    .    .    .    .    .    .    .
.    .    .    .    .    .    .    .    .    .
.    .    .    .    .    .    .    .    .    .
[at X{1}, Y{NG{2}] ... [at X{NG{1}}, Y{NG{2}}]
```

. . . . . .

. . . . . .

. . . . . .

at Z{NG{3}}, set NG{3} of the 3rd dimension:

[at X{1}, Y{1}] ... [at X{NG{1}}, Y{1}]

. . . . . .

. . . . . .

. . . . . .

[at X{1}, Y{NG{2}] ... [at X{NG{1}}, Y{NG{2}}]

. . . . . .

. . . . . .

. . . . . .

. . . . . .

. . . . . .

. . . . . .

at T{NG{4}}, set NG{4} of the 4th dimension:

at Z{1}, set 1 of the 3rd dimension:

[at X{1}, Y{1}] ... [at X{NG{1}}, Y{1}]

. . . . . .

. . . . . .

. . . . . .

[at X{1}, Y{NG{2}] ... [at X{NG{1}}, Y{NG{2}}]

at Z{2}, set 2 of the 3rd dimension:

[at X{1}, Y{1}] ... [at X{NG{1}}, Y{1}]

. . . . . .

. . . . . .

. . . . . .

[at X{1}, Y{NG{2}] ... [at X{NG{1}}, Y{NG{2}}]

. . . . . .

. . . . . .

. . . . . .

at Z{NG{3}}, set NG{3} of the 3rd dimension:

[at X{1}, Y{1}] ... [at X{NG{1}}, Y{1}]

. . . . . .

. . . . . .

. . . . . .

[at X{1}, Y{NG{2}] ... [at X{NG{1}}, Y{NG{2}}]

Explanation of A Virtual Environment File Data Fields

The physical units associated with each parameter may be found in Table 3-2.

general virtual environment data:

[virtual environment geometry type, integer, Table 3-1]

virtual environment dimensions, reals:
[dimension 1] [dimension 2] [dimension 3]

[relative error limit, real]

[critical value for specific confidence level, real]

[NRD, number of mesh points for radiological data, integer]

corresponding energies of the mesh points, reals:
[energy{1}] . . . [energy{NRD}]

exposure dose conversion factor data, reals:
[data point{1}] . . . [data point{NRD}]

[NSRC, number of sources, integer]

[NSTR, number of structures, integer]

[NREC, number of receptors, integer]

[4D linking parameter, real]

data for the virtual objects follows next in the order of:
1) sources
2) structures
3) receptors

data for sources (repeat input 1 to NSRC):

[source geometry type, integer, Table 3-1]

source dimensions, reals:
[dimension 1] [dimension 2] [dimension 3]

source location in virtual environment coordinates, reals:
[x location] [y location] [z location]

source orientation with respect to virtual environment axis, reals:
[parameter 1] [parameter 2] [parameter 3]

[source density, real]

[NSRD, number of mesh points for radiological data, integer]

corresponding energies of the mesh points, reals:
[energy{1}] . . . [energy{NSRD}]

mass attenuation coefficients, reals:
[data point{1}] . . . [data point{NSRD}]

Berger buildup parameter alpha, reals:
[data point{1}] . . . [data point{NSRD}]

Berger buildup parameter beta, reals:
[data point{1}] . . . [data point{NSRD}]

[total source activity, real]

[NE, number of different source gamma ray energies, integer]

corresponding energies of the gammas, reals:
[energy{1}] . . . [energy{NE}]

gamma-ray energy probabilities per decay, reals:
[fraction{1}] . . . [fraction{NE}]

data for structures (repeat input 1 to NSTR):

[structure geometry type, integer, Table 3-1]

structure dimensions, reals:
[dimension 1] [dimension 2] [dimension 3]

structure location in virtual environment coordinates, reals:
[x location] [y location] [z location]

structure orientation with respect to virtual environment axis, reals:
[parameter 1] [parameter 2] [parameter 3]

[structure density, real]

[NORD, number of mesh points for radiological data, integer]

corresponding energies of the mesh points, reals:
[energy{1}] . . . [energy{NORD}]

mass attenuation coefficients, reals:
[data point{1}] . . . [data point{NORD}]

Berger buildup parameter alpha, reals:
[data point{1}] . . . [data point{NORD}]

Berger buildup parameter beta, reals:
[data point{1}] . . . [data point{NORD}]

data for receptors (repeat input 1 to NREC):

receptor location in virtual environment coordinates, reals:
[x location] [y location] [z location]

[material dose conversion factor, real]

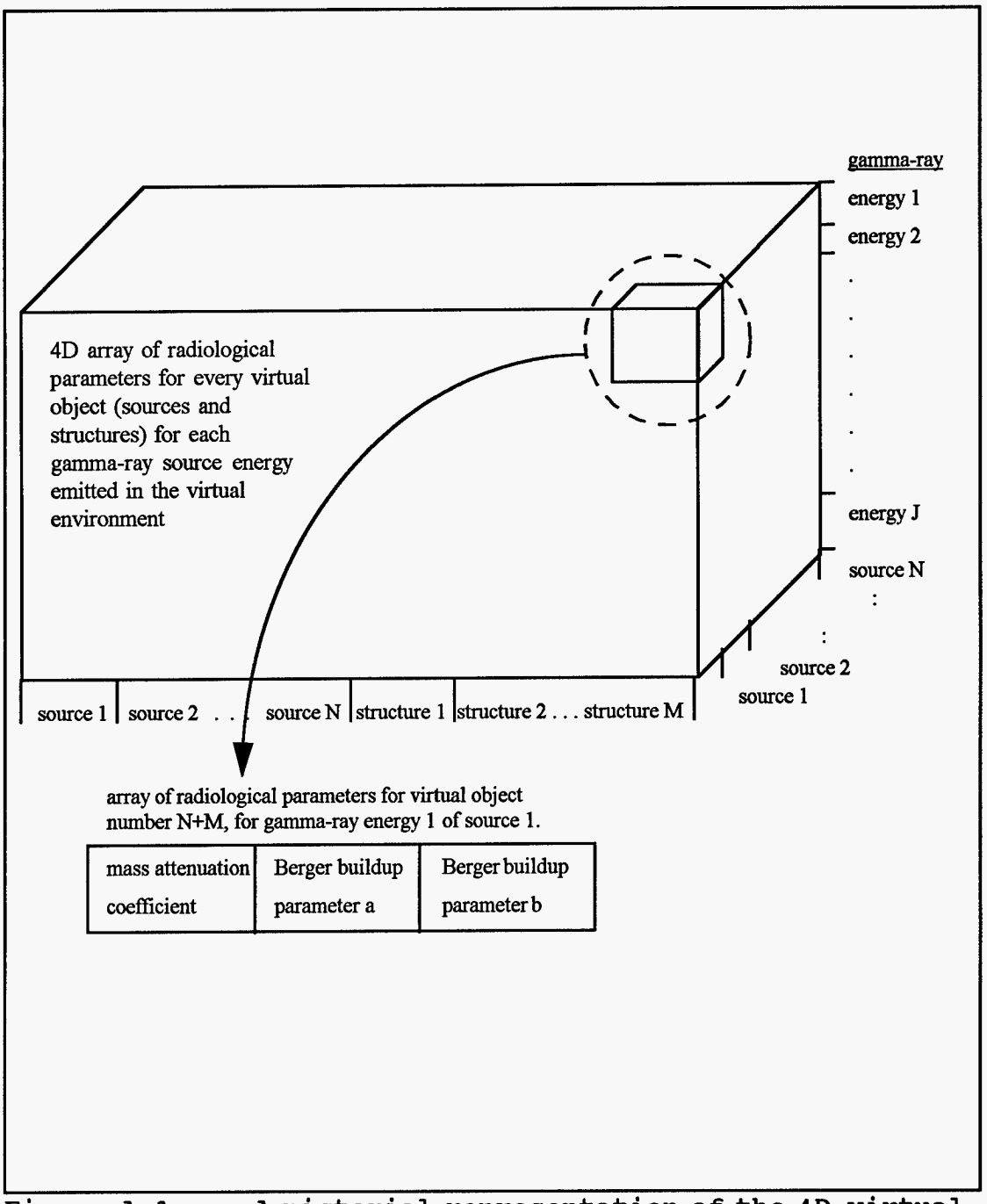

Figure A-1. A pictorial representation of the 4D-virtual-object-radiological-data array. Each element of the 3D array shown is itself a 1D array of data for a particular object for a particular source energy.

BIOGRAPHICAL SKETCH

Travis Warren Knight graduated as Salutatorian from Union County High School in June 1988. From there, he attended Florida's flagship university, the University of Florida. There he was awarded a Bachelor of Science in Nuclear Engineering degree with honors in August 1994. To aid in his studies, Travis was fortunate to receive several scholarships including awards from the Florida Undergraduate Scholarship Fund and the Academy for Nuclear Training/INPO. While an undergraduate, Travis worked three semesters as a student engineer (co-op) at River Bend Nuclear Station in St. Francisville, Louisiana. Also, he served as an intern for the Integral Fast Reactor Program at Argonne National Laboratory-West in Idaho Falls, Idaho. Being awarded a Department of Energy Applied Health Physics Fellowship, he continued his studies at the University of Florida in the Department of Nuclear Engineering Sciences.

I certify that I have read this study and that in my opinion it conforms to acceptable standards of scholarly presentation and is fully adequate, in scope and quality, as a thesis for the degree of Master of Science.

G. R. Dalton, Chairman
Professor of Nuclear
Engineering Sciences

I certify that I have read this study and that in my opinion it conforms to acceptable standards of scholarly presentation and is fully adequate, in scope and quality, as a thesis for the degree of Master of Science.

J. S. Tulenko, Cochairman
Professor of Nuclear
Engineering Sciences

I certify that I have read this study and that in my opinion it conforms to acceptable standards of scholarly presentation and is fully adequate, in scope and quality, as a thesis for the degree of Master of Science.

W. Emmett Bolch
Professor of Environmental
Engineering Sciences

This thesis was submitted to the Graduate Faculty of the College of Engineering and to the Graduate School and was accepted as partial fulfillment of the requirements for the degree of Master of Science.

December, 1995

Winfred M. Phillips
Dean, College of
Engineering

Karen A. Holbrook
Dean, Graduate School

Report Number (14) DOE/OR/00033--T733

Publ. Date (11) 1995

Sponsor Code (18) DOE/EH, XF

UC Category (19) UC-600, DOE/ER

DOE